# Journal Pre-proof


Development of submicromolar 17β-HSD10 inhibitors and their *in vitro* and *in vivo* evaluation

Ondrej Benek, Michaela Vaskova, Marketa Miskerikova, Monika Schmidt, Rudolf Andrys, Aneta Rotterova, Adam Skarka, Jana Hatlapatkova, Jana Zdarova Karasova, Matej Medvecky, Lukas Hroch, Lucie Vinklarova, Zdenek Fisar, Jana Hroudova, Jiri Handl, Jan Capek, Tomas Rousar, Tereza Kobrlova, Rafael Dolezal, Ondrej Soukup, Laura Aitken, Frank Gunn-Moore, Kamil Musilek

PII: S0223-5234(23)00559-7

DOI: https://doi.org/10.1016/j.ejmech.2023.115593

Reference: EJMECH 115593

To appear in: *European Journal of Medicinal Chemistry*

Received Date: 23 December 2022

Revised Date: 13 May 2023

Accepted Date: 23 June 2023

Please cite this article as: O. Benek, M. Vaskova, M. Miskerikova, M. Schmidt, R. Andrys, A. Rotterova, A. Skarka, J. Hatlapatkova, J.Z. Karasova, M. Medvecky, L. Hroch, L. Vinklarova, Z. Fisar, J. Hroudova, J. Handl, J. Capek, T. Rousar, T. Kobrlova, R. Dolezal, O. Soukup, L. Aitken, F. Gunn-Moore, K. Musilek, Development of submicromolar 17β-HSD10 inhibitors and their *in vitro* and *in vivo* evaluation, *European Journal of Medicinal Chemistry* (2023), doi: https://doi.org/10.1016/j.ejmech.2023.115593.

- Protein binding
- Enzyme inhibition

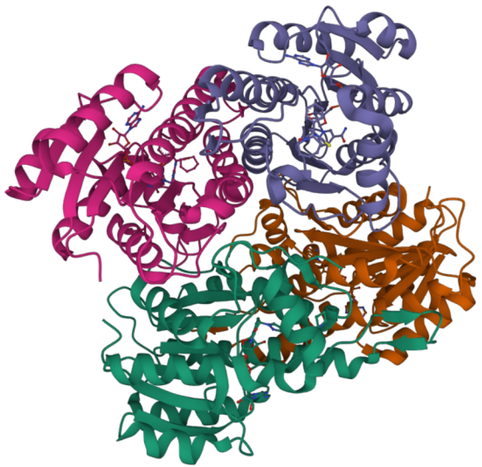

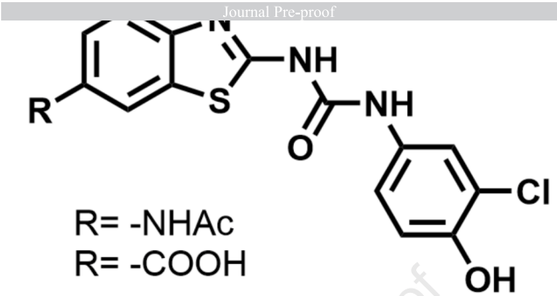


R= -NHAc
R= -COOH

- Pharmacokinetics

- Mitochondrial off-targets

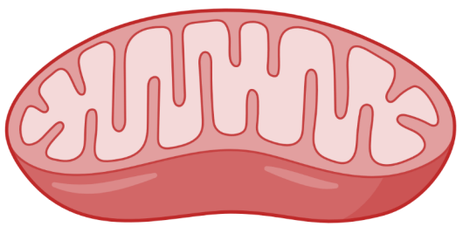

- Cytotoxicity

# Development of submicromolar 17β-HSD10 inhibitors and their *in vitro* and *in vivo* evaluation

Ondrej Benek[1,2*], Michaela Vaskova[1], Marketa Miskerikova[1], Monika Schmidt[1,2], Rudolf Andrys[1], Aneta Rotterova[1], Adam Skarka[1], Jana Hatlapatkova[3], Jana Zdarova Karasova[3], Matej Medvecky[1,4], Lukas Hroch[2], Lucie Vinklarova[1], Zdenek Fisar[5], Jana Hroudova[5], Jiri Handl[6], Jan Capek[6], Tomas Rousar[6], Tereza Kobrlova[2], Rafael Dolezal[2], Ondrej Soukup[2], Laura Aitken[7], Frank Gunn-Moore[7], Kamil Musilek[1,2*]

[1] *University of Hradec Kralove, Faculty of Science, Department of Chemistry, Rokitanskeho 62, 500 03 Hradec Kralove, Czech Republic*

[2] *University Hospital Hradec Kralove, Biomedical Research Centre, Sokolska 581, 500 05 Hradec Kralove, Czech Republic*

[3] *University of Defence, Faculty of Military Health Sciences, Department of Toxicology and Military Pharmacy, Trebesska 1575, 500 01, Hradec Kralove, Czech Republic*

[4] *University of Warwick, Bioinformatics Research Technology Platform, Coventry CV4 7AL, United Kingdom*

[5] *Charles University and General University Hospital in Prague, First Faculty of Medicine, Department of Psychiatry, Ke Karlovu 11, 120 00, Prague 2, Czech Republic*

[6] *University of Pardubice, Faculty of Chemical Technology, Department of Biological and Biochemical Sciences, Studentska 573, Pardubice 53210, Czech Republic*

[7] *University of St. Andrews, School of Biology, Biomedical Science Research Complex, North Haugh, St. Andrews KY16 9ST, United Kingdom*

* Correspondence: ondrej.benek@uhk.cz and kamil.musilek@uhk.cz

**Keywords:** amyloid-binding alcohol dehydrogenase (ABAD); Alzheimer's disease, 17β-hydroxysteroid dehydrogenase type 10 (17β-HSD10), enzyme inhibition, pharmacokinetics

**Highlights**

Fifteen new 17β-HSD10 inhibitors were designed, prepared, and evaluated.

Four submicromolar 17β-HSD10 inhibitors were identified (**6**, **9**, **11**, **12**).

Pharmacokinetic study after i.v. and p.o. administration was performed for **9** and **11**.

**Graphical Abstract** (Created with BioRender.com)

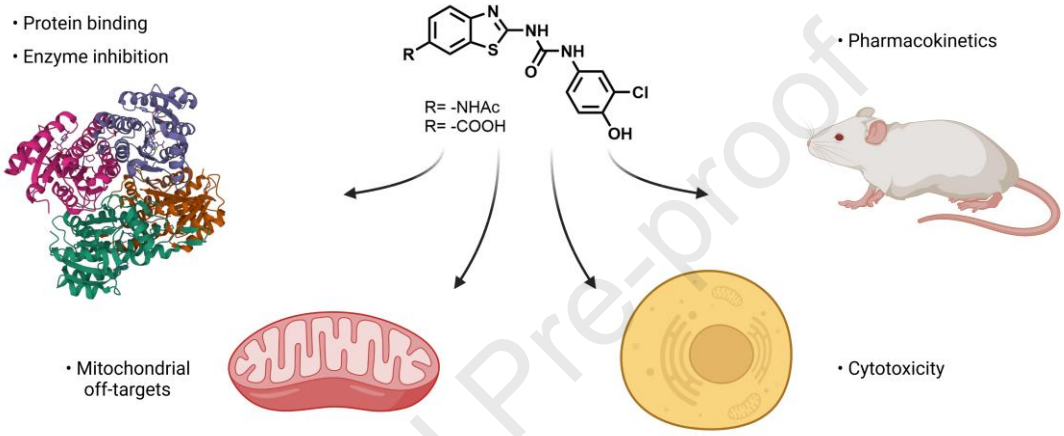


**Abstract**

17β-hydroxysteroid dehydrogenase type 10 (17β-HSD10) is a multifunctional mitochondrial enzyme and putative drug target for the treatment of various pathologies including Alzheimer's disease or some types of hormone-dependent cancer. In this study, a series of new benzothiazolylurea-based inhibitors were developed based on the structure-activity relationship (SAR) study of previously published compounds and predictions of their physico-chemical properties. This led to the identification of several submicromolar inhibitors ($IC_{50}$ ~0.3 µM), the most potent compounds within the benzothiazolylurea class known to date. The positive interaction with 17β-HSD10 was further confirmed by differential scanning fluorimetry and the best molecules were found to be cell penetrable. In addition, the best compounds weren´t found to have additional effects for mitochondrial off-targets and cytotoxic or neurotoxic effects. The two most potent inhibitors **9** and **11** were selected for *in vivo* pharmacokinetic study after intravenous and peroral administration. Although the pharmacokinetic results were not fully conclusive, it seemed that compound **9** was bioavailable after peroral administration and could penetrate into the brain (brain-plasma ratio 0.56).

## 1. Introduction

17β-hydroxysteroid dehydrogenase type 10 (17β-HSD10), also formerly termed amyloid-binding alcohol dehydrogenase (ABAD), is an oxidoreductase enzyme located in the mitochondrial matrix. It can catalyse the turnover of numerous substrates, especially steroids and neurosteroids. Besides its catalytic activity, it also acts as a structural component of RNase P. Thus, it is involved in many physiological functions. 17β-HSD10 plays an important role in the development of several human diseases and its inhibition is considered a potential treatment strategy for Alzheimer's disease (AD) and hormone-dependent cancer [1].

The development of AD is connected with an elevated level of amyloid-β peptide (Aβ), tauopathy, and mitochondrial dysfunction in the brain [2]. There are several putative mechanisms of Aβ toxicity to neuronal cells [3]. One of the theories focuses on the detrimental effects of Aβ on mitochondrial functions via interaction with mitochondrial proteins. Among other mitochondrial targets, Aβ is known to interact with 17β-HSD10, which compromises its function and contributes to mitochondrial dysfunction seen in AD. Blocking the interaction of 17β-HSD10 with Aβ or inhibition of 17β-HSD10 enzymatic function suppresses Aβ toxicity and ameliorates mitochondrial dysfunction, and thus presents a potential AD treatment strategy [1,4,5].

Due to its important role in steroid metabolism, 17β-HSD10 is implicated in some cancer types. In prostate cancer, 17β-HSD10 enables steroid synthesis, catalysing the alternative synthesis pathway of androgen by generating dihydrotestosterone (DHT) in the absence of testosterone [6,7]. It was also suggested that 17β-HSD10 overexpression supports cancer growth and makes the cancer cells more resistant to oxidative stress [8,9]. Based on these findings, inhibition of 17β-HSD10 could be considered a potential treatment strategy for cancer [1,7].

There is only a limited number of 17β-HSD10 inhibitors known to date. Based on their structure, the inhibitors can be sorted into three main classes, i.e., pyrazoles [10,11], steroids [7,12,13], and benzothiazolylureas. Benzothiazolylureas and their analogues are the largest class of 17β-HSD10 inhibitors and their development was described in a number of studies [14–22]. The most potent benzothiazolylurea inhibitors known to date (**1** – **5**) have $IC_{50}$ values ~1 μM (Figure 1) [21,22].

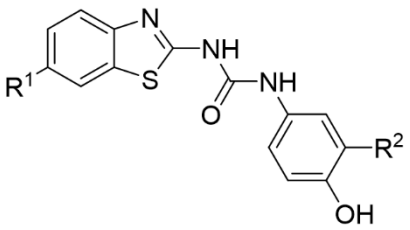


| Compound | $R^1$ | $R^2$ | $IC_{50}$ (μM) |
|---|---|---|---|
| **1** | OMe | Br | 1.3 |
| **2** | OEt | Cl | 1.6 |
| **3** | $SO_2Me$ | Cl | 0.9 |
| **4** | OH | Cl | 1.2 |
| **5** | $NH_2$ | Cl | 1.6 |

**Figure 1:** The most potent benzothiazolylurea 17β-HSD10 inhibitors discovered to date (**1** – **5**).

The intention of this study was to design and develop new benzothiazolylurea inhibitors with improved activity and/or physico-chemical properties that would be suitable for *in vivo* experiments.

## 2. Results and Discussion

### 2.1 Structural Design

Formerly, our research group has published several articles on the development of 1-benzothiazolyl-3-phenylurea 17β-HSD10 inhibitors [17–22]. SAR analysis of previous results highlighted several key structural motifs important for inhibition activity. Firstly, the 3-halogen-4-hydroxy substitution pattern on phenyl moiety was crucial for potent enzyme inhibition [17,18,21,22]. It seems that halogens, with their electron-withdrawing inductive (-I) effect, could increase the acidity and/or hydrogen bond donor (HBD) capacity of the neighbouring hydroxyl group, which resulted in improved binding and inhibition. However, electron-withdrawing groups with negative mesomeric (-M) effect (e.g., carboxyl, carbonyl) were not tolerated except for the nitrile group. This could be due to their ability to create an intramolecular hydrogen bond with the neighbouring hydroxyl group while creating a 6-membered ring. This would result in a decreased acidity/HBD capability of the neighbouring hydroxyl, which consequently manifested in the lower activity of the corresponding inhibitor. In contrast, the nitrile group (-M effect) possess linear geometry, thus could not form a hydrogen bond with the neighbouring hydroxyl. To further probe this theory, we decided to prepare compounds **6** and **7** (Figure 2A) substituted with strongly electron-withdrawing trifluoromethyl group (-I effect) and nitro group (-M effect, the potential for intramolecular H-bonding), respectively.

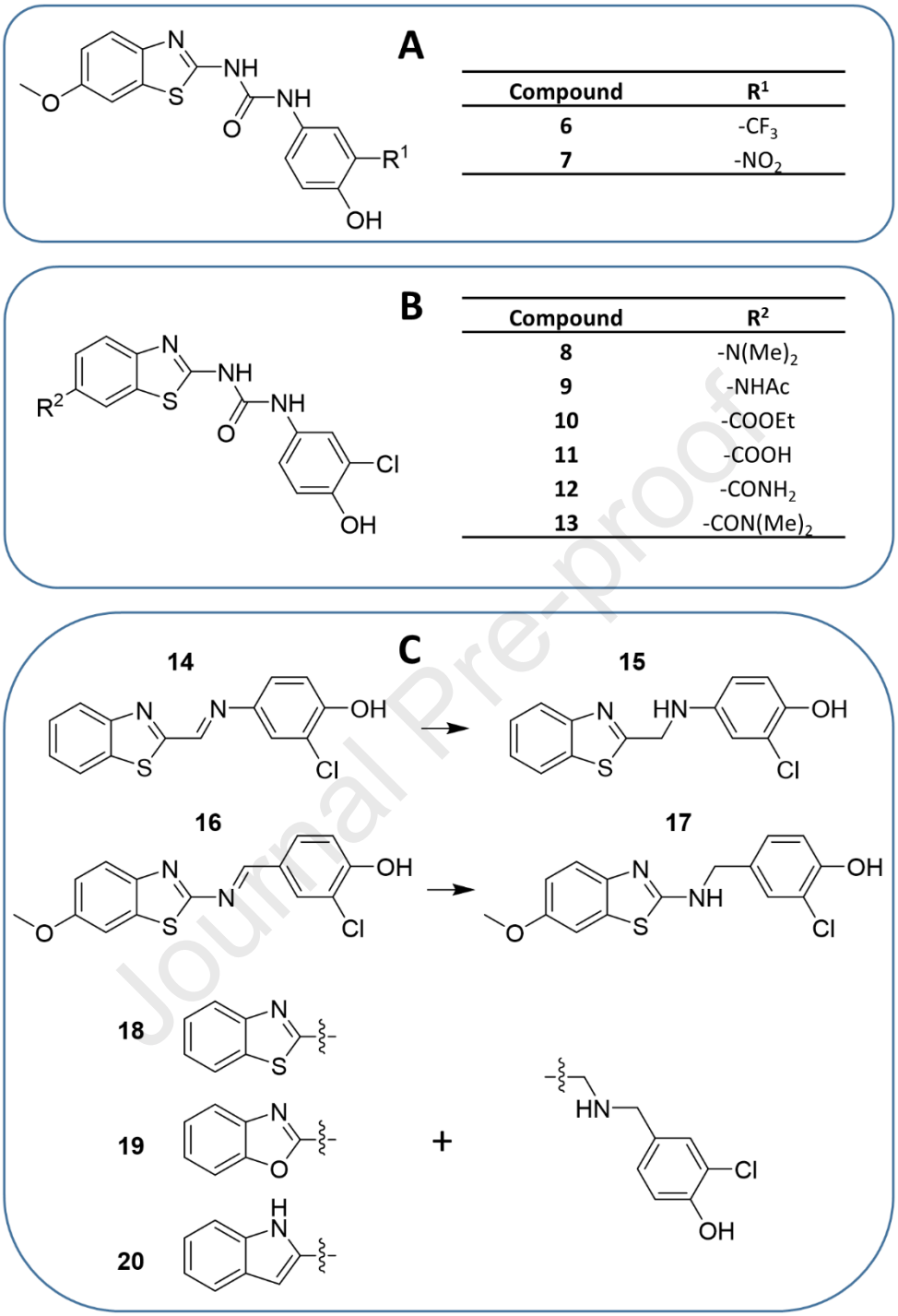


**Figure 2:** Prepared compounds could be divided into three series. **A**) Compounds **6** and **7** with halogen in position 3 of phenyl moiety replaced with alternative electron-withdrawing groups. **B**) Compounds **8** – **13** with different substitutions in position 6 of benzothiazolyl moiety. **C**) Compounds **14** – **20** with non-urea linkers.

Secondly, the substitution in position 6 of benzothiazolyl moiety affected the inhibition potency. The best-known inhibitors bear either a larger HBA group (ethoxy in compound **2**, methanesulfonyl in **3**) or a small HBD group (hydroxyl in **4** and primary amine in **5**) [21,22]. Therefore, we decided to prepare a series of compounds containing larger substituents with combined HBA/HBD properties (Figure 2B). Further, the synthetic precursor of compound **11** (ester **10**) was also isolated and evaluated. To assess the importance of HBD properties, we prepared *N*-methylated analogues of **5** and **12** devoid of HBD character (compounds **8** and **13**, respectively; Figure 2B).

The ability to pass cell membranes is a necessary pre-requisite for drugs acting via intracellular effectors (e.g., 17β-HSD10). The ability to pass cell membranes (via passive diffusion) can be assessed by *in silico* predictions of their physico-chemical properties. Even more strict physico-chemical criteria are required from CNS-targeted drugs that need to pass blood–brain barrier (BBB) to exert their effect in the brain [23,24]. Thus, we have calculated the physico-chemical properties [25] of the designed compounds and used the CNS multiparameter optimization (MPO) developed by Wager et al. [23] to predict and compare the likeliness of BBB-permeation. As can be seen, the benzothiazolylureas have rather suboptimal physico-chemical properties with the exception of compounds **7** and **12** (Table 1).

**Table 1:** Calculated physico-chemical properties of new inhibitors. MPO score ≥ 4 indicates that the compound is likely to be CNS bioavailable.

| Compound | Clog*P* | Clog*D* | TPSA | MW | HBD | p$K_a$ | MPO | Clog$S_{7.4}$ |
|---|---|---|---|---|---|---|---|---|
| optimal score | ≤ 3 | ≤ 2 | 40-90 | ≤ 360 | ≤ 0.5 | ≤ 8 | 4-6 | ≥ (-4) |
| **6** | 3.92 | 3.57 | 111.72 | 383.35 | 3 | 2.31 | 3.0 | -4.86 |
| **7** | 2.97 | 1.97 | 157.54 | 360.35 | 3 | 2.22 | 4.2 | -4.13 |
| **8** | 3.90 | 3.74 | 105.73 | 362.83 | 3 | 3.6 | 3.3 | -4.86 |
| **9** | 2.82 | 2.29 | 131.59 | 376.82 | 4 | 1.72 | 3.7 | -4.06 |
| **10** | 4.18 | 2.95 | 128.79 | 391.83 | 3 | 0.38 | 2.9 | -3.95 |
| **11** | 3.44 | -0.16 | 139.79 | 363.78 | 4 | 0.38 | 3.8 | -1.36 |
| **12** | 2.36 | 1.27 | 145.58 | 362.79 | 5 | 0.52 | 4.0 | -3.43 |
| **13** | 2.79 | 1.67 | 122.80 | 390.84 | 3 | 0.69 | 3.9 | -3.98 |
| **14** | 4.35 | 4.32 | 73.72 | 288.75 | 1 | 1.79 | 4.2 | -4.86 |
| **15** | 4.17 | 4.16 | 73.39 | 290.77 | 2 | 2.94 | 3.9 | -4.55 |
| **16** | 4.02 | 3.36 | 82.95 | 318.78 | 1 | 3.91 | 4.6 | -3.77 |
| **17** | 3.90 | 3.84 | 82.62 | 320.79 | 2 | 3.83 | 4.1 | -4.72 |
| **18** | 3.61 | 3.58 | 73.39 | 304.80 | 2 | 5.46 | 4.4 | -2.87 |
| **19** | 3.06 | 3.02 | 58.29 | 288.73 | 2 | 6.33 | 5.0 | -2.88 |
| **20** | 3.67 | 1.71 | 48.05 | 286.76 | 3 | 9.24 | 4.2 | -1.63 |

**Notes:** *In silico* predictions of physico-chemical properties using ACS Percepta software. The multiparameter optimization (MPO) scoring function is based on six fundamental physico-chemical parameters – calculated

partition coefficient (Clog*P*); calculated distribution coefficient at pH 7.4 (Clog*D*); molecular weight (MW); topological polar surface area (TPSA); number of HBD; most basic centre (p$K_a$). All properties are weighted equally, with a desirability score ranging from 0.0 to 1.0 and therefore a total CNS MPO desirability score ranges from 0.0 to 6.0. The MPO score for CNS available drugs is ≥ 4. Further, aqueous solubility at pH 7.4 was predicted (Clog$S_{7.4}$).

To address this issue, we have designed compounds with urea linker replaced by two- or three-membered aliphatic linker (compounds **15**, **17**, and **18**; Figure 2C) and benzothiazolyl moiety replaced by isosteric benzoxazole or indole heterocycles (compounds **19** and **20**; Figure 2C). Further, two imine precursors, **14** and **16,** were also isolated and evaluated (Figure 2C). All the "non-urea" compounds, with the exception of **15** (MPO = 3.9), comply with the MPO score for CNS bioavailable drugs (MPO ≥ 4; Table 1). In addition, solubility is another important physico-chemical parameter predictive for BBB penetration, with most CNS drugs having aqueous solubility at pH 7.4 higher than 100 µmol/L [24]. The previously published urea inhibitors showed, in some cases, low solubility, which hampered theirs *in vitro* assessment [18]. Therefore, we have accounted for solubility when designing the non-urea compounds. As seen in Table 1, compounds **17** – **20** have improved Clog$S_{7.4}$ values compared to urea compounds (with the exception of likely highly soluble compound **11**).

### 2.2 Synthesis

Compounds containing urea linker in their structure were generally prepared via a two-step synthesis. Firstly, the corresponding benzothiazole-2-amine was treated with 1,1'-carbonyldiimidazole to form an imidazolyl intermediate, which was then treated with the corresponding aniline derivative to yield the 1,3-disubstituted urea as a final product. Final product **11** substituted in position 6 of benzothiazole with carboxyl group was prepared via basic hydrolysis of ethyl ester **10** (Figure 3).

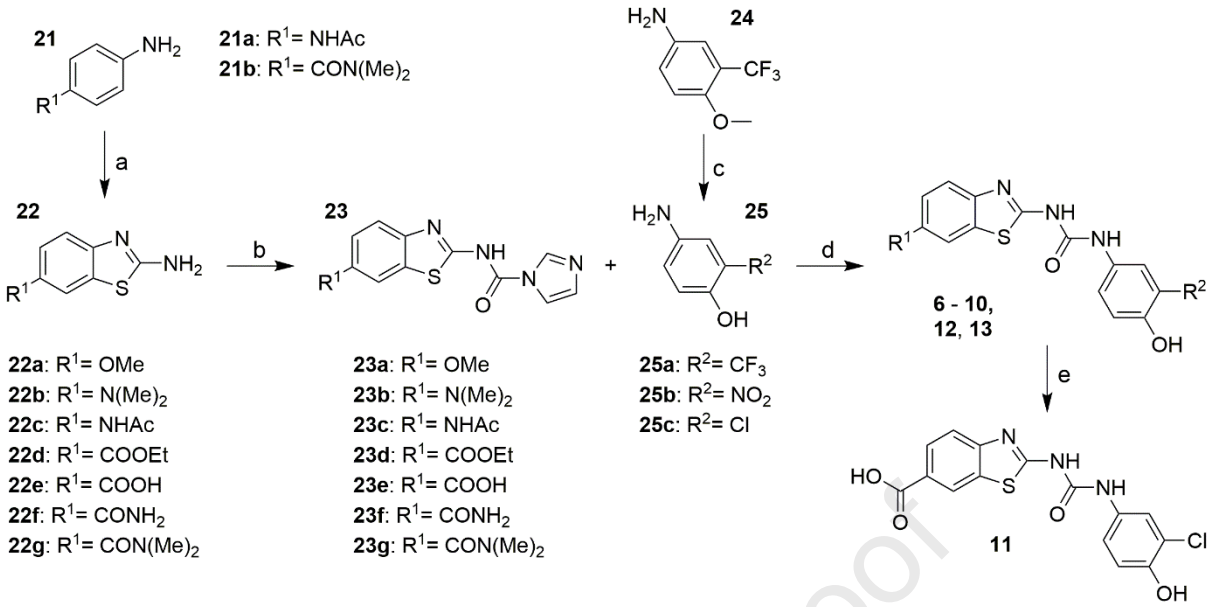


**Figure 3:** General method for synthesis of 1-(benzo[*d*]thiazol-2-yl)-3-phenylurea derivatives **6** – **13**. Reagents and conditions: (a) KSCN, tetramethylammonium dichloroiodate(I), DMSO/$H_2O$, RT – 70 °C; (b) CDI, DCM, RT; (c) HBr, acetic acid, reflux; (d) MeCN, reflux; (e) NaOH, $H_2O$/MeOH, 50 °C.

In several cases, the required 2-aminobenzothiazole and 4-aminophenol precursors were not commercially available, thus, they were synthesized. 4-amino-2-(trifluoromethyl)phenol (**25a**) was prepared by de-methylation of 4-methoxy-3-(trifluoromethyl)aniline using hydrobromic acid (Figure 3). Benzothiazole-2-amines substituted in position 6 with acetamide (**22b**) or dimethylcarboxamide group (**22g**) were prepared from corresponding *para*-substituted anilines in reaction with potassium thiocyanate and tetramethylammonium dichloroiodate(I) (Figure 3).

However, using above-mentioned process didn't yield desired $N^6$,$N^6$-dimethylbenzo[*d*]thiazole-2,6-diamine (**30**). Therefore, it was prepared from 6-nitrobenzo[*d*]thiazole-2-amine via 4-step synthesis (Figure 4). Firstly, the amine group of 6-nitrobenzo[*d*]thiazole-2-amine was protected with di-*tert*-butyl dicarbonate. Secondly, the nitro group was reduced with Pd/C catalysed hydrogenation. Consequently, the 6-amine group was di-methylated with methyl iodide, and finally, *N*-Boc acidic deprotection yielded $N^6$,$N^6$-dimethylbenzo[*d*]thiazole-2,6-diamine.

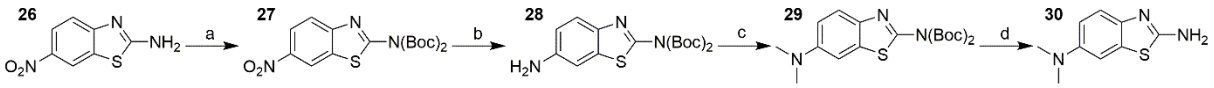


**Figure 4:** Synthesis of $N^6$,$N^6$-dimethylbenzo[*d*]thiazole-2,6-diamine (**30**). Reagents and conditions: (a) $(Boc)_2O$, DMAP, THF, RT; (b) Pd/C, $H_2$, EtOH, RT; (c) methyl iodide, $K_2CO_3$, DMF, RT; (d) 4M HCl, dioxane, RT.

Inhibitors with two-membered aliphatic linker (**15**, **17**) were prepared from corresponding aldehyde and amine starting materials via reductive amination. Imine intermediates **14** and **16** were also isolated and evaluated (Figure 5).

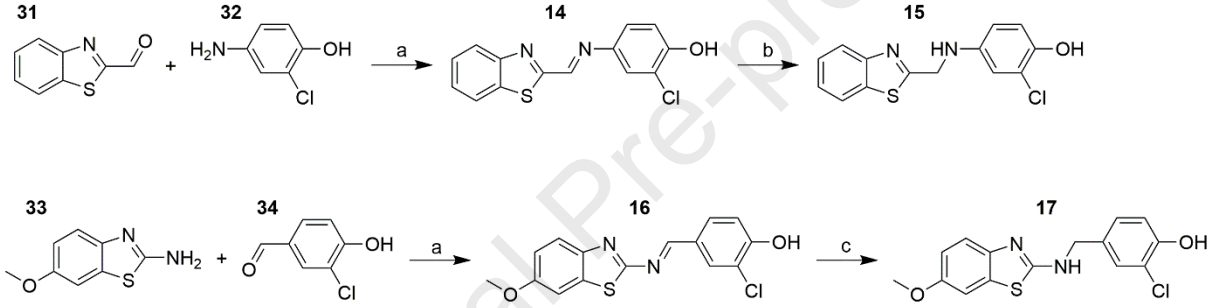


**Figure 5:** Synthesis of inhibitors with two-atom linkers. Reagents and conditions: (a) toluene, reflux; (b) Pd/C, MeOH, RT; (c) $NaBH_4$, MeOH, RT.

Benzothiazole derivative with three-membered aliphatic linker (**18**) was prepared in two steps via nucleophilic substitution from 2-(bromomethyl)benzo[*d*]thiazole and (3-chloro-4-methoxyphenyl)methanamine and by consequent de-methylation of methoxy group from the resulting intermediate (Figure 6). The corresponding benzoxazole derivative (**19**) was prepared in three steps (Figure 6). First, 2-aminophenol was converted to 2-(chloromethyl)benzo[*d*]oxazole in reaction with 2-chloroacetyl chloride. Then, 2-(chloromethyl)benzo[*d*]oxazole reacted with 4-(aminomethyl)-2-chlorophenol to obtain 1-(benzo[*d*]oxazol-2-yl)-*N*-(3-chloro-4-methoxybenzyl)methanamine, which was consequently de-methylated to obtain final product **19**. The corresponding indole derivative (**20**) was prepared in two steps. Reductive amination of 1*H*-indole-2-carbaldehyde and (3-chloro-4-methoxyphenyl)methanamine yielded the methoxy intermediate that was consequently de-methylated to obtain compound **20** (Figure 6).

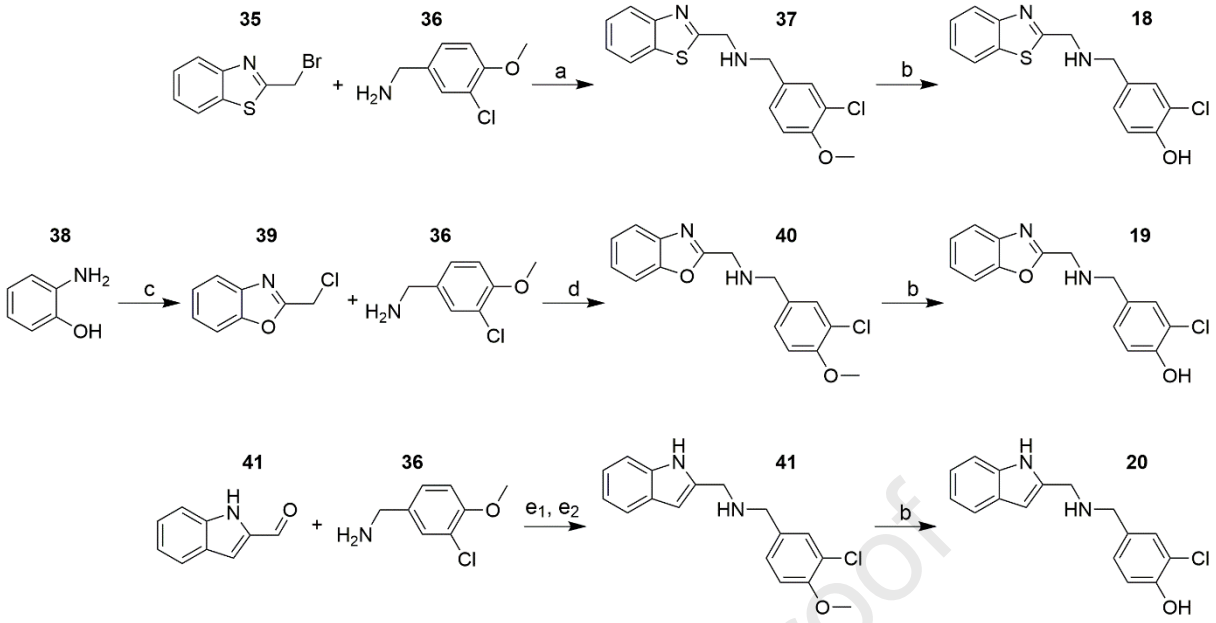


**Figure 6:** Synthesis of inhibitors with three-atom aliphatic linkers (**18** – **20**). Reagents and conditions: (a) DIEA, DCM, RT; (b) $AlCl_3$; DCE, 60°C; (c) 2-chloroacetyl chloride, $Et_3N$, *o*-xylene, 145°C; (d) DIEA, MeCN, 70°C; ($e_1$) MeOH, 0°C – RT; ($e_2$) $NaBH_3CN$, MeOH, 0°C – RT.

The details of chemical synthesis are described in the Experimental Section of the manuscript (Chapter 4). All final products were characterized by $^{1}H/^{13}C$ NMR and HRMS techniques (spectral data are provided in the Supporting Information).

### 2.3 Experimental Physico-chemical Parameters

To validate the predicted physico-chemical properties of prepared compounds, we have measured the log*P*, log*D*, p$K_a$, and log$S_{7.4}$ values (Table 2). The distribution coefficient of prepared compounds between water – octanol (log*P*) and PBS buffer (pH 7.4) – octanol (log*D*) was determined by UHPLC-DAD-MS measurement of analyte concentration in a particular solvent. The negative decimal logarithms of the dissociation constants (p$K_a$) of prepared compounds were determined spectrophotometrically using buffers of given pH (range from 3.0 to 11.5 with 0.5-unit increment).

**Table 2:** Experimental physico-chemical properties of prepared compounds.

| Compound | log*P* | log*D* | p$K_a$ | log$S_{7.4}$ |
|---|---|---|---|---|
| **6** | 4.28 ± 0.05 | 5.06 ± 0.24 | 11.23 ± 0.33 | -4.48 |
| **7** | 3.47 ± 0.01 | 3.44 ± 0.01 | 10.43 ± 0.14 | -4.78 |
| **8** | 4.09 ± 0.03 | 4.08 ± 0.05 | 4.61 ± 0.11 | -4.08 |
| **9** | 3.66 ± 0.19 | 3.35 ± 0.09 | 9.83 ± 0.06 | -4.55 |
| **10** | 4.58 ± 0.02 | 4.64 ± 0.02 | 9.26 ± 0.18 | -4.81 |
| **11** | 1.19 ± 0.01 | 0.75 ± 0.10 | 9.75 ± 0.23 | -4.36 |
| **12** | 3.32 ± 0.05 | 3.34 ± 0.12 | 9.35 ± 0.05 | -4.78 |
| **13** | 2.94 ± 0.01 | 2.95 ± 0.08 | 9.51 ± 0.15 | -4.81 |
| **14** | 2.94 ± 0.03 | 2.73 ± 0.06 | 9.14 ± 0.14 | -4.68 |
| **15** | 3.77 ± 0.02 | 3.88 ± 0.04 | 9.07 ± 0.04 | -4.69 |
| **16** | 3.79 ± 0.04 | 3.95 ± 0.01 | 11.57 ± 0.02 | -4.73 |
| **17** | 4.19 ± 0.03 | 4.17 ± 0.03 | 8.40 ± 0.08 | -4.73 |
| **18** | 4.03 ± 0.05 | 4.04 ± 0.01 | 8.79 ± 0.14 | -3.99 |
| **19** | 3.14 ± 0.06 | 3.19 ± 0.02 | 8.74 ± 0.21 | -3.38 |
| **20** | 2.84 ± 0.06 | 2.73 ± 0.10 | 7.60 ± 0.06 | -3.39 |

Generally, the *in silico* predictions of log*P*, log*D*, and log$S_{7.4}$ correlated plausibly with the experimental results, showing similar trends when comparing the compounds. However, the experimental values were generally shifted in a less-desired direction (i.e., higher log*P* and log*D*, and lower log$S_{7.4}$ values). The p$K_a$ (most basic center) measurements were limited by the assay pH window 3–12, as most urea derivatives were predicted to have p$K_a$ less than 3. Therefore, the comparison was possible only for urea **8** and non-urea compounds **16 – 20**. However, the predicted and experimental values did not correlate very well, showing the limitations in the prediction of p$K_a$ for this particular set of compounds. Taken together, the experimental measurement of physico-chemical parameters confirmed that the non-urea compounds generally had better "CNS drug-like" properties than their urea counterparts and, thus, are more likely to penetrate the BBB.

### 2.4 Enzyme Inhibition

The prepared compounds were initially screened for their inhibition activity towards 17β-HSD10 at 10 µM concentration (Table 3). Compounds that showed inhibition higher than 50 % (i.e., residual activity lower than 50 % of uninhibited enzymatic reaction) were consequently forwarded for 1 µM screening. Compounds that showed inhibition higher than 40 % at 1 µM (i.e., residual activity lower than 60 %) were consequently forwarded for $IC_{50}$ measurement. $K_i$ values were calculated from $IC_{50}$ data using method by Cer et al. [26].

**Table 3:** Results of 17β-HSD10 inhibition screening, $IC_{50}$ measurements, and $K_i$ calculations.

| Compound | 17β-HSD10 inhibition | | | | | |
|---|---|---|---|---|---|---|
| | **10 µM screening** Residual activity (%) | ***p* value*** | **1 µM screening** Residual activity (%) | ***p* value*** | **$IC_{50}$** (µM) | **$K_i$#** (µM) |
| control | 100 ± 4.3 | | 100 ± 4.8 | | | |
| **6** | 13.0 ± 2.4 | <0.0001 | 39.8 ± 4.5 | <0.0001 | 0.57 ± 0.12 | 0.44 |
| **7** | 79.4 ± 2.8 | 0.0022 | | | | |
| **8** | 27.0 ± 1.4 | <0.0001 | 62.7 ± 8.0 | 0.0023 | | |
| **9** | 22.0 ± 3.4 | <0.0001 | 49.5 ± 9.9 | 0.0014 | 0.34 ± 0.07 | 0.25 |
| **10** | 58.6 ± 2.1 | 0.0001 | | | | |
| **11** | 17.5 ± 4.0 | <0.0001 | 50.0 ± 11.4 | 0.0022 | 0.31 ± 0.09 | 0.23 |
| **12** | 38.3 ± 2.1 | <0.0001 | 50.0 ± 6.2 | 0.0004 | 0.84 ± 0.18 | 0.65 |
| **13** | 31.0 ± 2.1 | <0.0001 | 70.0 ± 11.2 | 0.013 | | |
| **14** | 68.7 ± 4.0 | 0.0008 | | | | |
| **15** | 72.1 ± 4.8 | 0.0017 | | | | |
| **16** | 76.6 ± 2.9 | 0.0014 | | | | |
| **17** | 33.2 ± 5.2 | <0.0001 | 74.4 ± 9.0 | 0.0122 | | |
| **18** | 54.1 ± 1.4 | <0.0001 | | | | |
| **19** | 67.6 ± 5.0 | 0.001 | | | | |
| **20** | 73.8 ± 3.2 | 0.0011 | | | | |

**Notes:** All reactions were measured in triplicate, and the values are expressed as mean ± SD.

* Versus control by Student's *t*-test.

# Values calculated based on the models described in Cer et al. (2009) [26].

Out of fifteen new compounds, four were found to be highly potent inhibitors with submicromolar $IC_{50}$ values (namely **6**, **9**, **11** and **12**). The most potent inhibitors **9** and **11** had $IC_{50}$ of 0.34 µM and 0.31 µM, respectively. Unfortunately, none of the non-urea compounds have been found very active in the 10 µM screening except compound **16**, which advanced for the 1 µM screen, but it did not advance further for $IC_{50}$ measurement.

From the structure-activity point of view, we have identified or verified several important features that affect inhibitory activity. Replacement of chlorine in position 3 of phenyl moiety with trifluoromethyl (compound **6**) led to a significant increase in activity compared to fluorinated and chlorinated analogues (presented in Schmidt et al. [22]). Nitro-substituted analogue **7**, on the other hand, was found inactive. This complies with our theory that this position is ideal for an electron-withdrawing substituent that, at the same time, cannot create an intramolecular H-bond to neighbouring hydroxyl, so that the hydroxyl stays available for H-bonding (as a H-bond donor) or eventually salt-bridge interaction with the target enzyme. The other three potent (submicromolar) inhibitors bear an HBD group at position 6 of benzothiazolyl moiety (acetamide **9**, carboxyl **11,** and amide **12**), while analogues devoid of HBD character (dimethylamine **8**, ester **10**, and dimethylamide **13**) were found less potent.

Finally, replacing of the urea linker with a two- or three-membered linker led to a decrease in activity (analogic ureas presented in Schmidt et al. [22]).

### 2.5 Molecular docking

The molecular docking study was performed with two different protein structures (PDB: 1E6W and 1U7T) and using two docking softwares (AutoDock: Vina [27] and MOE [28]). The docking was performed with all the prepared compounds, so that calculated binding energies (Table 4) could be compared to experimental inhibition data. Further, the inspection of ligands orientation within the active site and their binding interactions with protein residues were studied. The key findings were demonstrated for the most potent inhibitor out of each of the three structural series (Figure 2), i.e. compound **6** for class A, compound **11** for class B and compound **17** for class C (Figures 7). A 2D depiction of individual ligands within the active site can be found in Supporting Information (Figures S1, S2, S3).

The best correlation between estimated binding energy and inhibition results was obtained for 1E6W receptor using MOE (Table 4). In this setup, the urea-linked compounds (**6**-**13**) performed better to non-urea analogues. Similar trend, though less pronounced, was observed also for MOE with 1U7T receptor. On the other hand, results from AutoDock: Vina (AD: Vina) with either receptor did not pick up this trend. However, none of the docking setups could predict the differences in inhibitor potency in regard to different substitutions of benzothiazolyl of phenyl moieties. Resulting Gibbs binding energies from AD: Vina with 1U7T receptor correctly predicted compounds **6**, **11** and **17** as the best hits within their structural series, while they showed lower binding energy values for other two highly active compounds **9** and **12**.

**Table 4:** Calculated binding energies in various docking setups (receptor 1E6W or 1U7T; docking software AD: Vina or MOE).

| Compound | Binding energy estimate [kcal/mol] | | | |
|---|---|---|---|---|
| | AD: Vina | | MOE | |
| | 1U7T | 1E6W | 1U7T | 1E6W |
| **6** | -7,3 | -6,6 | -6 | -7,1 |
| **7** | -6,8 | -5,9 | -6,1 | -7,2 |
| **8** | -6,0 | -1,9 | -6,1 | -7 |
| **9** | -6,3 | -1,2 | -6,6 | -7,1 |
| **10** | -6,5 | -1,6 | -6,3 | -7,6 |
| **11** | -6,9 | -6,7 | -6 | -6,8 |
| **12** | -6,5 | -2,3 | -5,8 | -7,1 |
| **13** | -6,4 | 0,4 | -6,3 | -7,6 |
| **14** | -6,1 | -5,6 | -5 | -5,9 |
| **15** | -6,4 | -7,0 | -5,7 | -6,5 |
| **16** | -6,4 | -3,5 | -5,6 | -6,2 |
| **17** | -6,7 | -7,1 | -5,7 | -6,8 |
| **18** | -6,2 | -7,5 | -6 | -6,4 |
| **19** | -6,3 | -7,4 | -5,8 | -7,1 |
| **20** | -6,6 | -7,8 | -5,6 | -6,6 |

The overall orientation of ligands within the binding site differed for AD: Vina and MOE as depicted for the exemplary inhibitors **6**, **11** and **17** (Figure 7). In MOE (both receptors) the urea linked compounds **6** and **11** were oriented with their phenyl moiety facing inside, towards the $NAD^+$ cofactor, while the benzothiazolyl moiety pointed towards entrance of the active site. On the other hand, compound **17** with aliphatic linker was oriented in opposite direction. This could possibly explain the better docking score as well as experimental inhibition results of urea-linked compounds (**6**-**13**) compared to non-urea analogues (**14**-**20**). In AD: Vina (both receptors), however, the orientation of the three sample inhibitors did not show any regular pattern offering no particular explanation for the experimental inhibition data.

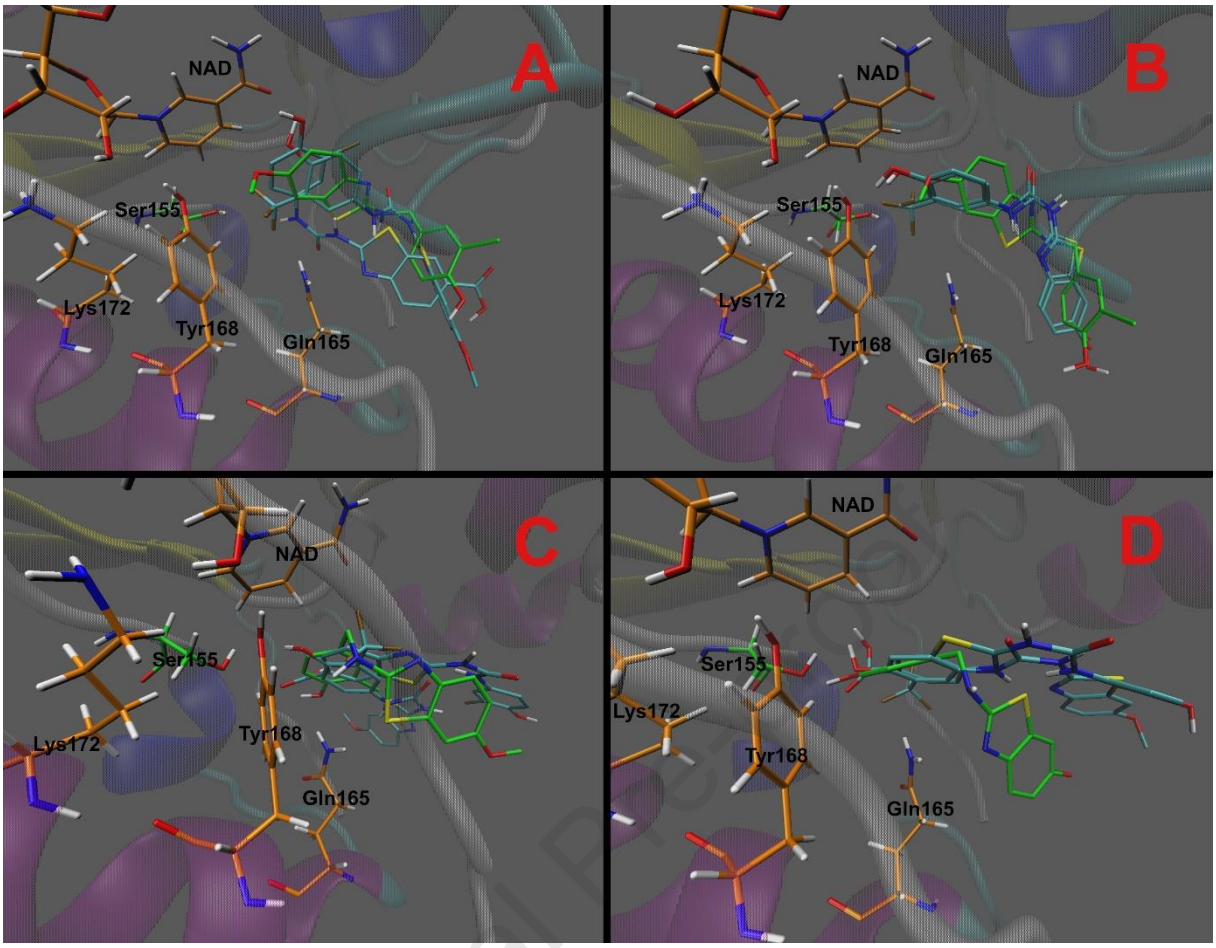


**Figure 7:** Superimposition of the top-scoring binding modes of compounds with **6**, **11** and **17** in 1E6W (A, C) and 1U7T (B, D) as predicted by MOE (A, B) and AD: Vina (C, D). Inhibitors **6** and **11** are shown in cyan, serine 155 residue along with inhibitor **17** are shown in green, other protein residues and $NAD^+$ cofactor are shown in orange.

Analysis of individual inhibitors and their interactions within the active site showed highly variable results and did not show any particular interaction responsible for good binding affinity/inhibition. Despite high variability of the ligand binding interactions, the docking results showed recurrent involvement of residues Gln162, Gln165, Lys212, Tyr168 as well as Ser155, especially if lower-scoring ligand poses were included in the analysis (see Figures 7, 8 and Supplementary Figures S1, S2, S3). Gln162 and Gln165 often showed van der Waals and possible H-bond interaction with NH or CO groups of the linker moiety. Lys212 showed either van der Waals or H-bond interaction with urea linker or phenyl ring substituents and also H-arene interaction with thiazolyl ring. Tyr168 and Ser155 from the catalytic site also seemed to frequently participate to ligand stabilization, although the nature of the interaction with ligands was not consistent. A specific interaction was frequently observed for inhibitor **11** - an H-bond between its carboxyl substituent and the C-terminal carboxyl of Pro261.

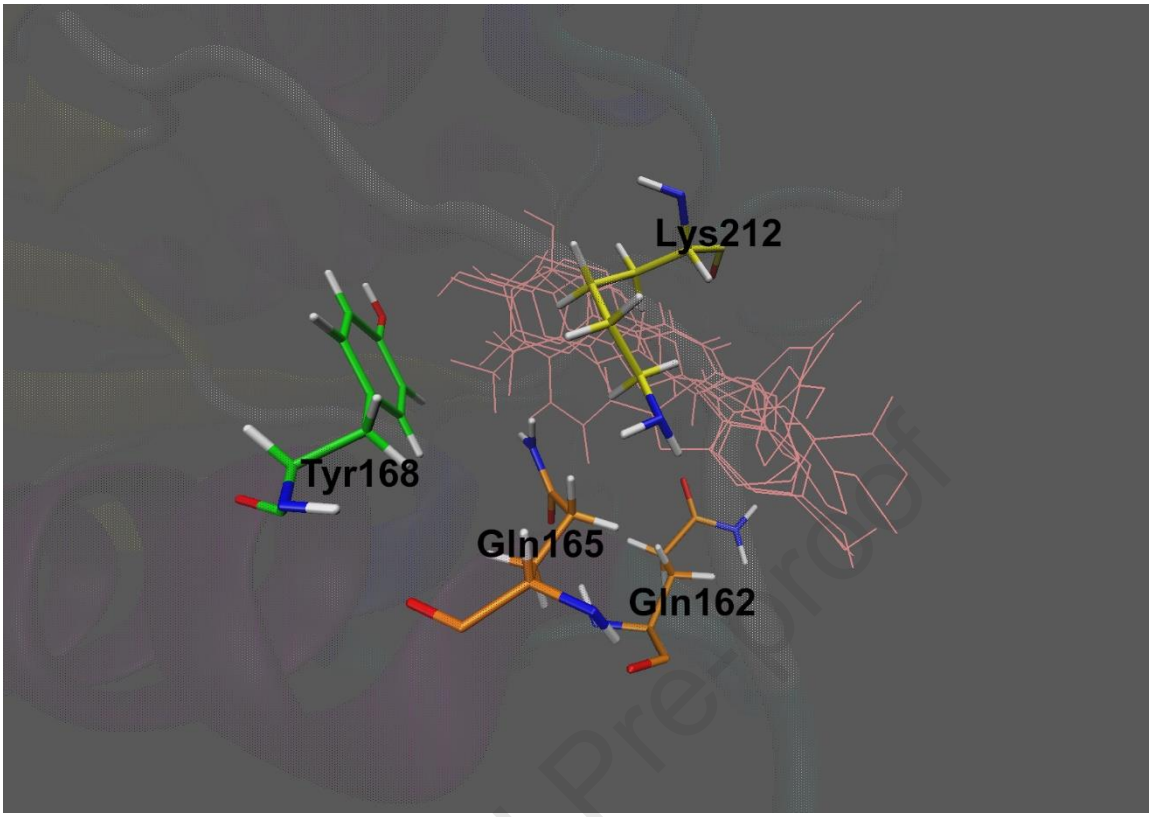


**Figure 8:** Residues that may play an important role in stabilization of ligands in the substrate-binding site of 17β-HSD10 enzyme (illustrated in 1E6W structure). The superimposed inhibitors are highlighted in pink.

Taken together, the docking results showed high variability in ligands orientation within the active site and in their interaction patterns with the particular amino acid residues, and thus the reliability of docking results seems rather low. An experimentally obtained 3D structure of a benzothiazolylurea inhibitor complexed together with 17β-HSD10 enzyme would be of great benefit for understanding the interactions that are taking place between this type of inhibitors and 17β-HSD10, thus providing a solid starting ground for the future docking studies.

### 2.6 Mitochondrial Off-targets

As the compounds are supposed to act on 17β-HSD10 within mitochondria, we assessed their effect on several potential mitochondrial off-targets, namely citrate synthase (CS), complexes I, II, and III of electron-transport chain, and monoamine oxidases A and B (MAO-A and MAO-B). For this evaluation, we have selected the four most potent 17β-HSD10 inhibitors **6**, **9**, **11**, and **12**.

The activity of mitochondrial CS, Complex I, and the couple Complex II+III was measured spectrophotometrically on isolated pig brain mitochondria at a drug concentration of 50 μM (Table 5). CS activity was measured as the colour change of 5,5'-dithiobis-(2-nitrobenzoic) acid (DTNB) according to a method published by Srere [29]. The activity of respiratory Complex I was measured based on the rotenone-sensitive rate of the NADH oxidation; a slightly modified previously published method [30] was used [31]. The Complex II+III activity was measured as the antimycin A-sensitive rate of cytochrome *c* reduction upon addition of succinate [32]. The activity of citrate synthase was not significantly affected by any tested compound. The activity of Complex I was inhibited significantly by three compounds (**6**, **9** and **12**). Complex II+III activity was partially inhibited by the compound **6** only. Thus, Complex I represents a potential off-target for these compounds, especially compound **6** (residual activity 5.3 % at 50 μM).

**Table 5:** Effects on citrate synthase and respiratory chain complexes activity at drug concentration of 50 μM.

| Compound | Citrate synthase activity (%) | *p* value* | Complex I activity (%) | *p* value* | Complex II+III activity (%) | *p* value* |
|---|---|---|---|---|---|---|
| control | 100.0 ± 5.5 | | 100.0 ± 3.3 | | 100.0 ± 5.6 | |
| **6** | 92.7 ± 0.3 | 0.0834 | 5.3 ± 7.5 | <0.0001 | 52.2 ± 8.7 | 0.0013 |
| **9** | 99.9 ± 0.1 | 0.9764 | 24.3 ± 7.1 | <0.0001 | 97.4 ± 1.1 | 0.4742 |
| **11** | 100.3 ± 0.3 | 0.9294 | 87.7 ± 12.3 | 0.1697 | ND | |
| **12** | 94.4 ± 5.4 | 0.2767 | 25.2 ± 18.1 | 0.0021 | 99.7 ± 9.5 | 0.9647 |

**Notes:** Values are expressed as mean ± SD for at least three independent measurements.
*Versus control by Student's *t*-test

The *in vitro* effects on the overall activity of the electron-transport chain (expressed as Complex I-linked respiration and Complex II-linked respiration) were measured using high-resolution respirometry as drug-induced changes in the oxygen consumption rate of the isolated mitochondria in state 3 respiration as described previously [33]. The obtained $IC_{50}$ values for all compounds were in the mid-micromolar range (Table 6), which was about two orders of magnitude higher than the $IC_{50}$ values

for inhibition of their primary target 17β-HSD10. The effects of the tested compounds on mitochondrial respiration are in good correlation with the above-mentioned effects on the activity of individual mitochondrial complexes, confirming that Complex I represents a potential off-target for compound **6**.

**Table 6:** Drug-induced inhibition of mitochondrial respiration.

| Compound | Complex I-linked respiration $IC_{50}$ (μM) | Complex II-linked respiration $IC_{50}$ (μM) |
|---|---|---|
| **6** | 28.0 ± 1.1 | 98 ± 19 |
| **9** | 36.4 ± 3.2 | 27 ± 47 |
| **11** | 93 ± 15 | 260 ± 143 |
| **12** | 88 ± 21 | ND* |

**Notes:** Mitochondrial respiration was measured in isolated pig brain mitochondria using protocols for the O2k-Respirometer (Oroboros). Inhibitory curves were analysed by the four-parameter logistic regression and the half-maximal inhibitory concentrations ($IC_{50}$) were established. Data are presented as mean ± standard error (SE) of at least three independent measurements.

*Compound **12** caused an increase in respiratory rate associated with Complex II.

The activities of MAO-A and MAO-B in isolated mitochondria were assayed using a radiochemical method by the modification of a previously published experimental protocol [34] with either radiolabelled serotonin ([$^3$H]5-HT) as the MAO-A substrate and radiolabelled phenylethylamine ([$^{14}$C]PEA) as the MAO-B substrate. The obtained $IC_{50}$ values for MAO-A and MAO-B (Table 7) were found in the mid-micromolar range except for the inhibition of MAO-A by compound **9** ($IC_{50}$ = 5.8 μM). Therefore, MAO-A should be considered a potential off-target for compound **9**, although its $IC_{50}$ value for 17β-HSD10 inhibition is still 10-times lower.

**Table 7:** Drug effects on monoamine oxidase (MAO) activity.

| Compound | MAO-A $IC_{50}$ (μM) | MAO-B $IC_{50}$ (μM) |
|---|---|---|
| **6** | 79 ± 17 | ND* |
| **9** | 5.8 ± 1.1 | 120 ± 23 |
| **11** | 85 ± 58 | 81 ± 8.9 |
| **12** | ND* | 84 ± 39 |

**Notes:** Monoamine oxidase (MAO) activity was assayed radiochemically in isolated pig brain mitochondria. Inhibitory curves were analysed by the four-parameter logistic regression and the half-maximal inhibitory concentrations ($IC_{50}$) were established. Data are presented as mean ± standard error (SE) of at least two independent measurements.

*Compounds **6** and **12** showed no inhibition for MAO-B and MAO-A, respectively.

Together, the tested compounds exhibited inhibitory effects on the activity of mitochondrial enzymes up to relatively high concentrations that mostly exceeded the expected therapeutic plasma concentrations. On the other hand, due to the positive effects of MAO-A inhibition on depression (frequent comorbidity in AD) and MAO-B inhibition on neurodegeneration [35], it may be actually appropriate to include the effect on MAO activity for novel AD lead molecules [36]. Targeting several pathological mechanisms with one molecule for the treatment of complex diseases like AD is a well-established approach, also termed as “multi-target drug design” [37]. Notably, compounds with a combined effect on 17β-HSD10 and MAOs had been previously developed by Hroch et al. [18].

### 2.7 Cytotoxicity and Cell Viability

A set of cellular assays was used to evaluate the cytotoxic potential of prepared compounds. Firstly, the four most potent inhibitors (**6**, **9**, **11**, **12**) were assessed for their toxic effects on HEK293 and SH-SY5Y cell lines. Cytotoxic effect and effect on cell viability were measured at two concentrations (1 and 10 μM) and expressed as normalized % of control values (1% DMSO and 100 μM valinomycin, respectively). The cell viability was determined as changes in ATP level by measuring luminescence in CellTitre-Glo® assay. The cytotoxicity of compounds was determined as changes in membrane integrity by measuring fluorescence in CellTox™ Green assay. None of the tested compounds showed significant toxicity at either concentration (Figure 9). A slight cytotoxic effect, as well as slightly decreased viability, were observed in both cell lines for compound **6** at 10 μM.

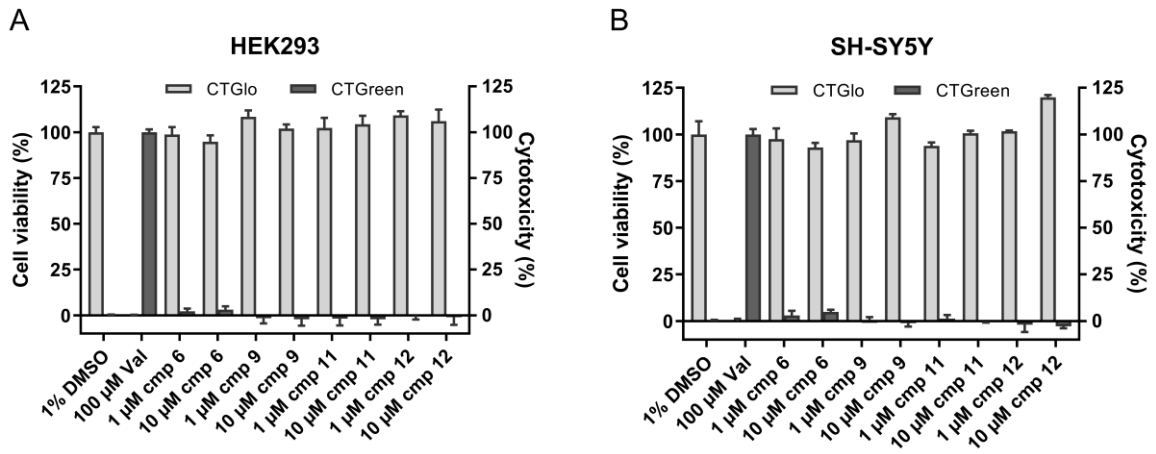


**Figure 9:** Cell viability and compound cytotoxicity determination. Cell viability was determined using CellTitre-Glo (Promega) in HEK293 (**A**) and SH-SY5Y (**B**) cell lines in multiplex with measurement of compounds cytotoxicity assayed by CellTox Green (Promega). Data are presented as mean ± standard error of at least two independent experiments in tetraplicate.

For further evaluation, we decided to discard compound **6**, due to its cytotoxicity and effects on mitochondrial off-targets, and also the less potent inhibitor **12**, and we continued with the two most promising compounds **9** and **11**. The cytotoxicity of the two most promising inhibitors was tested on neuronal cell line SH-SY5Y by measuring the glutathione levels (GSH assay) and dehydrogenase activity (WST-1 assay). The testing was performed at four concentrations (0.1 – 100 µM) and at two time-points (incubation for 4 and 24 hours). A significant decrease of glutathione levels was found only in cells treated with 100 µM compound **9** after 4 hours incubation, however, after 24 hours incubation this effect was less distinct (Figure 10A). Transient decrease of intracellular glutathione could be related to increased oxidative stress caused by incubation with tested compound. A significant decrease of dehydrogenase activity was found in cells treated with 100 µM compound **9** in both time intervals (Figure 10B). The decreased dehydrogenase activity of cells correlated with their decreased metabolic activity and viability. Notably, no signs of cytotoxicity were observed for compound **11**, even at the highest concentration tested. Taken together, the two most potent 17β-HSD10 inhibitors **9** and **11** showed low cytotoxicity up to 10µM concentration, when assessed via different methods and under various conditions, which is about two orders of magnitude above their $IC_{50}$ values for 17β-HSD10 inhibition. Additional cytotoxicity data were obtained via the lactate dehydrogenase (LDH) assay and can be found in the Supporting Information (Table S1).

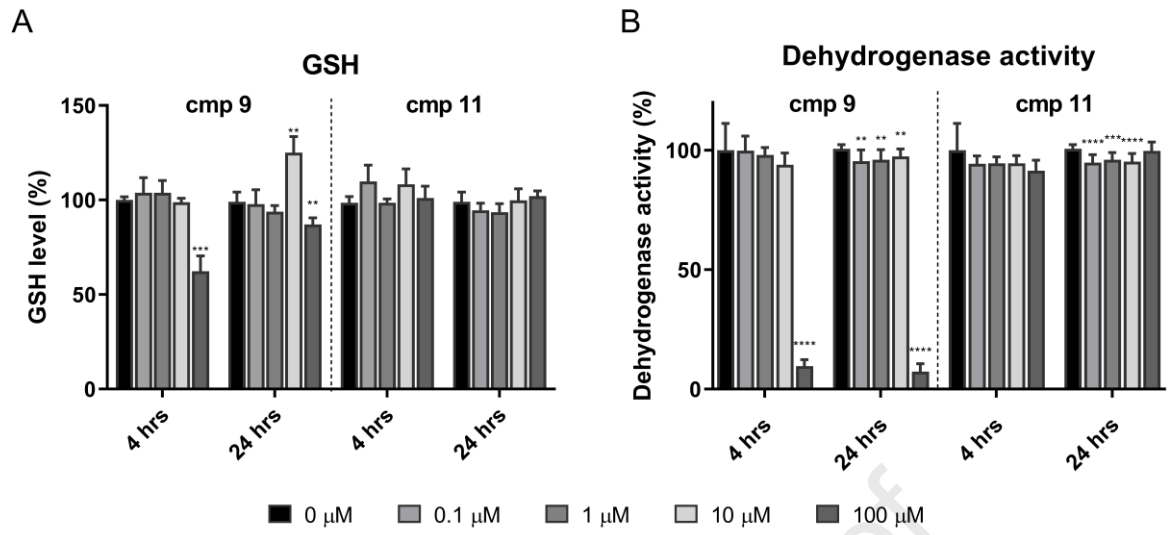


**Figure 10:** Effects of compounds on glutathione levels (**A**) and intracellular dehydrogenase activity (**B**). SH-SY5Y cells were incubated with inhibitors **9** and **11** (0.1 – 100 μM), for 4 and 24 hours. After treatment, dehydrogenase activity using WST-1 test and glutathione levels using monochlorobimane assay were measured. Data are presented as mean ± SD of triplicate of at least three independent experiments and differences between groups are determined by the Student's unpaired t-test. *$p \leq 0.05$, **$p \leq 0.01$, ***$p \leq 0.001$, ****$p \leq 0.0001$.

### 2.8 Differential Scanning Fluorimetry

Differential Scanning Fluorimetry (DSF) was employed as an orthogonal assay to confirm the best hits (**9**, **11**) identified in the enzymatic assay. DSF is used to detect the molecular binding between ligand and protein based on the change in the protein's denaturation temperature [38]. Both compounds significantly increased the denaturation temperature of the protein, and thus were confirmed to bind to the enzyme (Figure 11). The measurement was conducted at two different concentrations of the inhibitor, and the results were found concentration-dependent, which indicates specific binding (opposite to non-specific binding events based on ligand aggregation, etc.).

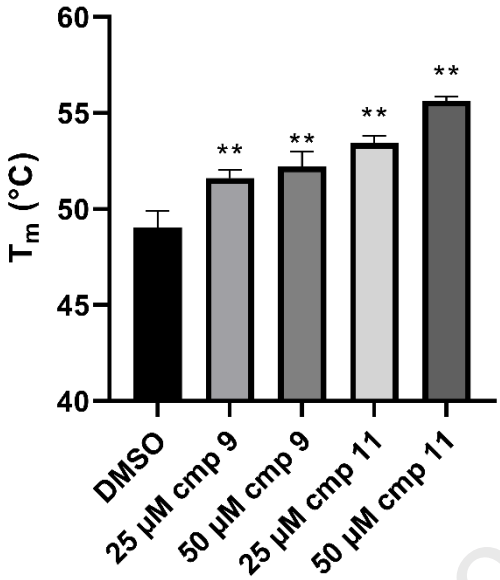


**Figure 11:** Results of DSF experiments. Inhibitors **9** and **11** were both found to interact with the protein, significantly increasing its denaturation temperature in a concentration-dependent manner. Values are given as means ± SD (n = 3) and differences between groups are determined by the Student's unpaired t-test. *$p \leq 0.05$, **$p \leq 0.01$, ***$p \leq 0.001$, ****$p \leq 0.0001$.

### 2.9 PAMPA-BBB

In order to further explore the capacity of the two most promising compounds **9** and **11** to penetrate into the brain, we used the Parallel Artificial Membrane Permeability Assay (PAMPA–BBB) described by Di et al. [39]. Further, we included the rather inactive compound **19**, which was however favoured for the BBB penetration by having the highest CNS-MPO score. An assay validation was made comparing the reported permeability values of commercial drugs. Based on the obtained results (Table 8) compounds **9** and **19** are expected to cross the BBB by passive diffusion, while compound **11** was predicted not to penetrate BBB.

**Table 8:** Prediction of BBB penetration of 17β-HSD10 inhibitors and standard drugs using PAMPA–BBB assay.

| Compound | BBB Penetration Estimation | |
|---|---|---|
| | Pe ± SEM (× $10^{-6}$ cm $s^{-1}$) | CNS (+/-) |
| **9** | 7.81 ± 1.00 | + |
| **11** | 0.39 ± 0.22 | - |
| **19** | 23.71 ± 5.41 | + |
| Furosemide | 0.19 ± 0.07 | - |
| Chlorothiazide | 1.15 ± 0.54 | - |
| Ranitidine | 0.35 ± 0.31 | - |
| Donepezil | 21.93 ± 2.06 | + |
| Tacrine | 5.96 ± 0.59 | + |
| Rivastigmine | 20.00 ± 2.07 | + |

**Notes:** 'CNS (+)' (high BBB permeability predicted); Pe ($10^{-6}$ cm·$s^{-1}$) > 4.0. 'CNS (−) (low BBB permeability predicted); Pe ($10^{-6}$ cm·$s^{-1}$) < 2.0. 'CNS (+/−) (BBB permeability uncertain); Pe ($10^{-6}$ cm·$s^{-1}$) from 4.0 to 2.0. Data are presented as the mean ± SEM of three independent measurements.

In correspondence to their physico-chemical properties and CNS-MPO score, compounds **11** and **19** showed positive and negative results in the PAMPA assay, respectively. Compound **19**, which obtained the highest CNS-MPO score, was also found superior in the PAMPA-BBB model with Pe value comparable with the best reference drugs donepezil and rivastigmine. On the other hand, compound **9** was found to be BBB permeable in PAMPA assay despite its calculated (Table 1) as well as experimentally determined (Table 2) physico-chemical properties did not fully meet the criteria suggested by CNS-MPO model.

### 2.10 Pharmacokinetics

Firstly, a pharmacokinetic study after intravenous (i.v.) administration was performed with compounds **9** and **11**. The 20μM solution of **9** or 25μM solution of **11** was applied to the tail-vein of male wild-type rats (0.1 mL per 100 g of weight = overall dose 0.013 mg/kg for **9** and 0.018 mg/kg for **11**). The inhibitors were dissolved in saline containing 3% DMSO, the dosing was based on the maximal solubility of compounds in water. Animals were sacrificed at 9 time-points (5, 15, 30, 60, 90, 180, 240, 360, and 1440 mins; 3 animals per time-point). Animals were exsanguinated, plasma and brain samples were collected, and the concentration of inhibitor in samples was quantified using HPLC-MS.

Consequently, pharmacokinetic study after peroral (p.o.) administration was performed with compounds **9** and **11**. The inhibitor was dissolved in a vehicle comprising of 10 % NMP, 25 % Kolliphor

EL and 65 % saline. The 16 mM inhibitor solution was applied with a blunt needle via the oesophagus into the stomach of male wild-type rats (overall dose 60 mg/kg). Animals were sacrificed at 15 time-points (5, 15, 30, 45, 60, 120, 180, 240, 300, 360, 420, 480, 540, 600, and 1440 mins; 3 animals per time-point). Animals were exsanguinated, plasma and brain samples were collected, and analysed by HPLC-MS. Treated animals (both administration routes) displayed normal behaviour without side effects for the entire period of experiments. The experimental data were analysed using standard non-compartmental analysis in the Kinetica software, version 4.0. The obtained results are summarized in Table 9.

**Table 9:** Pharmacokinetic parameters in plasma and brain following a single intravenous (dose 0.013 and 0.018 mg.kg$^{-1}$ for **9** and **11** respectively) and oral (dose: 60 mg.kg$^{-1}$) administration in male wild-type rats.

| **PLASMA (i.v.)** | **Compound 9** | **Compound 11** |
|---|---|---|
| $C_{max}$ (pM) | 389.00 ± 60.66 | 1540.33 ± 246.06 |
| $T_{max}$ (min) | 5.00 ± 0.00 | 5.00 ± 0.00 |
| $AUC_{0\text{-}1440}$ (min×pM) | 5 832 ± 895 | 18 961 ± 4 978 |
| $\lambda_z$ (L/min) | 0.049 ± 0.009 | 0.025 ± 0.003 |
| Half-life (min) | 15.80 ± 2.91 | 29.37 ± 3.74 |
| MRT (min) | 24.53 ± 3.76 | 15.70 ± 2.83 |
| CL (L/min/kg) | 6.67 ± 0.79 | 3.10 ± 0.62 |
| $V_z$ (L/kg) | 147.33 ± 26.92 | 134.97 ± 35.31 |
| **BRAIN (i.v.)** | **Compound 9** | **Compound 11** |
| $C_{max}$ (pM) | 12.61 ± 6.97 | 0.41 ± 0.34 |
| $T_{max}$ (min) | 956.00 ± 388.30 | 90.00 ± 0.00 |
| $AUC_{0\text{-}1440}$ (min×pM) | 3 299 ± 900 | 34.00 ± 28.00 |
| Kp brain (AUCbrain/AUCplasma) | 0.566 | 0.002 |
| **PLASMA (p.o.)** | **Compound 9** | **Compound 11** |
| $C_{max}$ (pM) | 13 529.33 ± 1 261.49 | 6 854.00 ± 923.33 |
| $T_{max}$ (min) | 35.00 ± 4.09 | 25.00 ± 4.09 |
| $AUC_{0\text{-}1440}$ (min×pM) | 1 431 047 ± 211 968 | 212 993 ± 30 083 |
| **BRAIN (p.o.)** | **Compound 9** | **Compound 11** |
| $C_{max}$ (pM) | 205.83 ± 124.37 | 154.33 ± 58.88 |
| $T_{max}$ (min) | 35.00 ± 4.09 | 40.00 ± 8.17 |
| $AUC_{0\text{-}1440}$ (min×pM) | 15 749 ± 7 917 | 20 135 ± 12 942 |
| Kp brain (AUCbrain/AUCplasma) | 0.011 | 0.095 |

**Notes:** $C_{max}$, maximal plasma or brain concentration; $T_{max}$, time to $C_{max}$; $AUC_{0\text{-}1440}$, area under curve/bioavailability; $\lambda_z$, elimination constant in terminal phase of curve, half-life in elimination phase; MRT, mean residence time; CL, clearance; $V_z$, elimination rate constant. All values are expressed as mean ± standard error (SE) of three independent measurements.

After i.v. administration, both compounds were successfully detected in plasma. Compound **11** was detected in higher concentrations and with higher AUC in plasma compared to **9**, otherwise both

compounds showed similar pharmacokinetic profiles. Regarding brain bioavailability after i.v. administration, compound **9** showed significantly higher exposure (0.57 brain/plasma ratio) compared to **11** (0.02 ratio), which was in accordance with the PAMPA assay (Table 8).

After p.o. administration, compound **9** reached a higher $C_{max}$ than **11** and had significantly higher AUC, while the $T_{max}$ values were similar for both compounds. Although the exact peroral bioavailability could not be assessed due to the different i.v. and p.o. dosage, it is obvious that compound **9** has a higher p.o. bioavailability compared to **11**. This is in agreement with the higher Pe value for compound **9** in the PAMPA assay and overall better physico-chemical properties, i.e. it is more likely to permeate through cellular membranes and absorb from the GIT. Regarding their $IC_{50}$ values, both compounds reached the effective concentration in plasma but only for a limited time (approx. 1 hour and 0.5 hour for **9** and **11,** respectively). Both compounds showed two plasma peaks after p.o. administration, which could indicate enterohepatic circulation. Contrary to i.v. results, the brain exposure was very low for both compounds after p.o. administration (less than 0.1 brain/plasma ratio), and their concentration did not reach effective levels, which would be a subject of further investigation.

## 3. Conclusion

Inhibition of mitochondrial enzyme 17β-HSD10 is a potential treatment strategy for AD or hormone-dependent cancer. In this study, we have developed a series of new benzothiazolylurea-based inhibitors. Several compounds were found to be submicromolar inhibitors and their interaction with 17β-HSD10 enzyme was further confirmed using DSF. Selected inhibitors **9** and **11** were extensively assessed *in vitro* and they were found non-cytotoxic up to high-micromolar concentrations, had good selectivity profile over potential mitochondrial off-targets, and compound **9** was predicted to pass BBB. Finally, a pharmacokinetic study of the two best inhibitors **9** and **11** was performed after i.v. and p.o. administration. While compound **11** showed an inappropriate pharmacokinetic profile, compound **9** was found to be perorally bioavailable and likely to penetrate to the brain, however, the brain bioavailability results were not fully conclusive, as brain penetration was observed only after i.v. but not after p.o. administration. Together, the *in vitro* and *in vivo* results highlighted compound **9** as a promising lead compound for further development and evaluation on animal models.

# 4. Experimental Section

## 4.1 General Chemistry

All reagents and solvents were purchased from commercial sources (Sigma Aldrich, Activate Scientific, Alfa Aesar, Merck, Penta Chemicals and VWR) and they were used without any further purification. Low boiling point (≥ 90% 40 – 60°C) petroleum ether (PE) was used if not stated otherwise. Thin-layer chromatography (TLC) for reaction monitoring was performed on Merck aluminium sheets, silica gel 60 $F_{254}$. Visualisation was performed either via UV (254 nm) or appropriate stain reagent solutions (alternatively in a combination of both). Preparative column chromatography was performed on silica gel 60 (70 – 230 mesh, 63 – 200 µm, 60 Å pore size). Melting points were determined on a Stuart SMP30 melting point apparatus and are uncorrected.

Nuclear magnetic resonance (NMR) spectra were acquired at 500/126 MHz ($^{1}$H, $^{13}$C) on a Varian S500 spectrometer or at 300/75 MHz ($^{1}$H and $^{13}$C) on a Varian Gemini 300 spectrometer. Chemical shifts δ are given in ppm and referenced to the signal center of solvent peaks (DMSO-$d_6$: δ 2.50 ppm and 39.52 ppm for $^{1}$H and $^{13}$C, respectively; Chloroform-*d*: δ 7.26 ppm and 77.16 ppm for $^{1}$H and $^{13}$C, respectively), thus indirectly correlated to TMS standard (δ 0 ppm). Coupling constants are expressed in Hz. Spectra acquisitions were performed by assoc. prof. Jiri Kunes workgroup, Department of Inorganic and Organic Chemistry, Faculty of Pharmacy in Hradec Kralove, Charles University in Prague.

High-resolution mass spectra (HRMS) were recorded by coupled LC-MS system consisting of Dionex UltiMate 3000 analytical LC system and Q Exactive Plus hybrid quadrupole-orbitrap spectrometer. As an ion-source, heated electro-spray ionization (HESI) was utilised (setting: sheath gas flow rate 40, aux gas flow rate 10, sweep gas flow rate 2, spray voltage 3.2 kV, capillary temperature 350°C, aux gas temperature 300°C, S-lens RF level 50. Positive ions were monitored in the range of 100 – 1500 m/z with the resolution set to 140 000. Obtained mass spectra were processed in Xcalibur 3.0.63 software.

## 4.2 Chemical Synthesis

**4-Amino-2-(trifluoromethyl)phenol (25a)**

4-Methoxy-3-(trifluoromethyl)aniline (1 eq) was dissolved in glacial acetic acid (3 mL/mmol) and hydrobromic acid (40%, 3 mL/mmol). The reaction mixture was heated at reflux for the next 20 h. The solution was neutralised with saturated $NaHCO_3$ solution. The aqueous layer was extracted with EtOAc (3 × 25 mL). Combined organic layers were washed with brine, dried over anhydrous $Na_2SO_4$ and the solvent was removed under reduced pressure. The crude residue was purified by column chromatography ($CHCl_3$:MeOH, 30:1) to yield 4-amino-2-(trifluoromethyl)phenol as an off-white solid (65 %).

$^1$H NMR (500 MHz, DMSO-$d_6$) δ 9.30 (s, 1H), 6.75 – 6.70 (m, 2H), 6.67 (dd, *J* = 8.6, 2.6 Hz, 1H), 4.95 (br s, 2H); HRMS (ESI) calcd for $C_7H_7F_3NO$ $[M+H]^+$ 178.0474, found 178.0473.

**Procedure A (general conditions): 6-substituted-benzo[*d*]thiazol-2-amines (22b, 22g)**

*N*-(4-Aminophenyl)acetamide or 4-amino-*N*,*N*-dimethylbenzamide (1 eq) and potassium thiocyanate (7 eq) were dissolved in DMSO:water (5 mL/mmol, 9:1) and stirred for 15 minutes. Tetramethylammonium dichloroiodate(I) (3 eq) was added and the reaction mixture was heated at 70°C for 16 h [40]. The reaction mixture was diluted with $H_2O$, alkalized with 1M NaOH and extracted with EtOAc (3 × 25 mL). Organic layers were combined, dried over anhydrous $Na_2SO_4$ and the solvent was removed under reduced pressure. The residue was recrystallized ($Et_2O$:EtOAc) to obtain 6-(substituted)benzo[*d*]thiazol-2-amine.

***N*-(2-Aminobenzo[*d*]thiazol-6-yl)acetamide (22b)**

Beige solid; yield 89 %; $^1$H NMR (500 MHz, DMSO-$d_6$) δ 9.86 (s, 1H), 8.00 (t, *J* = 1.3 Hz, 1H), 7.33 (s, 2H), 7.25 – 7.22 (m, 2H), 2.02 (s, 3H).

**2-Amino-*N*,*N*-dimethylbenzo[*d*]thiazole-6-carboxamide (22g)**

Beige solid; yield 81 %; $^1$H NMR (500 MHz, DMSO-$d_6$) δ 7.74 (d, *J* = 1.5 Hz, 1H), 7.64 (s, 2H), 7.32 (d, *J* = 8.2 Hz, 1H), 7.26 (dd, *J* = 8.2, 1.6 Hz, 1H), 2.96 (s, 6H).

***N*,*N*-di(Boc)-6-nitrobenzo[*d*]thiazol-2-amine (27)**

The mixture of 6-nitrobenzo[*d*]thiazol-2-amine (1 eq) and DMAP (0.05 eq) in anhydrous THF (5 mL/mmol) was cooled to 0°C and the solution of *tert*-butyl-dicarbonate (2.05 eq) in anhydrous THF (2 mL/mmol) was added drop-wise. The reaction mixture was allowed to reach RT, stirred overnight and heated at 65°C for 2 h to complete the reaction [41]. The solvent was removed under reduced pressure, the residue was diluted with EtOAc (25 mL), washed with citric acid (15%, 2 × 5 mL), water (5 mL) and brine (5 mL). The organic layer was dried over anhydrous $Na_2SO_4$, the solvent was removed under reduced pressure and the crude residue was subsequently recrystallized (PE:$Et_2O$) to yield *N*,*N*-di(Boc)-6-nitrobenzo[*d*]thiazol-2-amine as a light yellow solid (97 %).

$^1$H NMR (500 MHz, DMSO-$d_6$) δ 9.11 (d, *J* = 2.4 Hz, 1H), 8.29 (dd, *J* = 8.9, 2.4 Hz, 1H), 7.92 (d, *J* = 8.9 Hz, 1H), 1.57 (s, 18H).

***N*$^2$,*N*$^2$-di(Boc)-benzo[*d*]thiazole-2,6-diamine (28)**

*N*,*N*-di(Boc)-6-nitrobenzo[*d*]thiazol-2-amine (27; 1 eq) was dissolved in EtOH (10mL/mmol) and palladium on activated carbon (Pd/C, 10%, 0.05 eq) was added. The hydrogen atmosphere was

introduced and the mixture was stirred at RT overnight [42]. The mixture was filtered through cellite pad and evaporated to dryness. The crude product was subsequently recrystallized (PE:$Et_2O$) to yield $N^2$,$N^2$-di(Boc)-benzo[*d*]thiazole-2,6-diamine as a white solid (97 %).

$^1$H NMR (500 MHz, DMSO-$d_6$) δ 7.48 (d, *J* = 8.7 Hz, 1H), 7.01 (d, *J* = 2.2 Hz, 1H), 6.73 (dd, *J* = 8.7, 2.2 Hz, 1H), 5.36 (s, 2H), 1.48 (s, 18H).

**$N^2$,$N^2$-di(Boc)-$N^6$,$N^6$-dimethylbenzo[*d*]thiazole-2,6-diamine (29)**

The mixture of $N^2$,$N^2$-di(Boc)-benzo[*d*]thiazole-2,6-diamine (28; 1 eq), methyl iodide (2.05 eq) and potassium carbonate (2.05 eq) in DMF (5 mL) was stirred at RT overnight. The reaction mixture was diluted with $H_2O$, filtered and the crude residue was purified by column chromatography (heptane:EtOAc) to yield $N^2$,$N^2$-di(Boc)-$N^6$,$N^6$-dimethylbenzo[*d*]thiazole-2,6-diamine as a colourless oil (38 %).

$^1$H NMR (500 MHz, DMSO-$d_6$) δ 7.62 (d, *J* = 8.9 Hz, 1H), 7.25 (d, *J* = 2.5 Hz, 1H), 6.94 (dd, *J* = 9.0, 2.5 Hz, 1H), 2.95 (s, 6H), 1.49 (s, 18H).

**$N^6$,$N^6$-Dimethylbenzo[*d*]thiazole-2,6-diamine (30)**

$N^2$,$N^2$-di(Boc)-$N^6$,$N^6$-dimethylbenzo[*d*]thiazole-2,6-diamine (29; 1 eq) was stirred for 24 h in 4M HCl-dioxane solution (10 mL/mmol) [41]. The reaction mixture was diluted with $Et_2O$ (50 mL) to achieve complete hydrochloride salt precipitation, which was collected by suction filtration. The solution of 1 M NaOH was added to the mixture of hydrochloride salt in $H_2O$ to achieve a neutral pH value and the mixture was stirred for the next 2 h. Finally, the precipitate was collected by suction filtration, dried and recrystallized (PE:$Et_2O$) to yield $N^6$,$N^6$-dimethylbenzo[*d*]thiazole-2,6-diamine as a white solid (95 %).

$^1$H NMR (500 MHz, DMSO-$d_6$) δ 7.17 (d, *J* = 8.8 Hz, 1H), 7.05 (d, *J* = 2.6 Hz, 1H), 7.03 (s, 2H), 6.70 (dd, *J* = 8.8, 2.6 Hz, 1H), 2.83 (s, 6H).

**Procedure B (general conditions): *N*-(6-substituted-benzo[*d*]thiazol-2-yl)-1*H*-imidazole-1-carboxamides (23a-23g)**

*N*,*N*′-Carbonyldiimidazole (1.2 eq) was added to a solution of 6-substituted-benzo[*d*]thiazol-2-amine (1 eq) in anhydrous DCM (5 mL/mmol) and the reaction was heated at reflux for 20 h. The reaction mixture was cooled down to 2 – 8°C, the precipitate was collected by suction filtration and washed with cold DCM [154]. The crude product was dried under reduced pressure to yield *N*-(6-substituted-benzo[*d*]thiazol-2-yl)-1*H*-imidazole-1-carboxamide as a white solid and used in the next reaction step without further purification.

**Procedure C (general conditions): 1-aryl-3-(6-(substituted)benzo[*d*]thiazol-2-yl)ureas (6 – 10, 12, 13)**

An aniline derivative (1.1 eq) was added to the suspension of *N*-(6-substituted-benzo[*d*]thiazol- 2-yl)-1*H*-imidazole-1-carboxamide (1 eq) in anhydrous acetonitrile (15 mL/mmol) and the reaction was heated at reflux for 20 h [154]. The reaction was cooled to RT, quenched with 1 M HCl (15 mL/mmol) and the precipitate was collected by filtration. The crude product was recrystallized from $Et_2O$:MeOH and dried to constant weight yielding the corresponding 1-aryl-3-(6-substituted-benzobenzo[*d*]thiazol-2-yl)ureas (**6** – **10**, **12**, **13**).

**1-(4-Hydroxy-3-(trifluoromethyl)phenyl)-3-(6-methoxybenzo[*d*]thiazol-2-yl)urea (6)**

White solid; yield 64 %; m.p. 260.5 – 262.5 °C; $^1$H NMR (500 MHz, DMSO-$d_6$) δ 10.35 (br s, 1H), 9.74 (s, 1H), 7.74 (s, 1H), 7.55 (d, *J* = 9.0 Hz, 1H), 7.51 (s, 1H), 7.47 (d, *J* = 9.1 Hz, 1H), 7.03 (d, *J* = 8.9 Hz, 1H), 6.98 (d, *J* = 9.1 Hz, 1H), 3.79 (s, 3H); $^{13}$C NMR (126 MHz, DMSO-$d_6$) δ 157.77, 155.77, 152.25, 151.45, 141.75, 132.25, 129.91, 124.82, 123.91 (q, *J* = 270.5 Hz), 119.85, 117.49, 117.15 (q, *J* = 5.3 Hz), 115.17 (q, *J* = 30.3 Hz), 114.49, 105.01, 55.66; HRMS (ESI) calcd for $C_{16}H_{13}F_3N_3O_3S$ $[M+H]^+$ 384.0624, found 384.0611.

**1-(4-Hydroxy-3-nitrophenyl)-3-(6-methoxybenzo[*d*]thiazol-2-yl)urea (7)**

Beige solid; yield 99 %; m.p. 263 – 264.5 °C; $^1$H NMR (500 MHz, DMSO-$d_6$) δ 10.90 (s, 2H), 9.26 (s, 1H), 8.22 (d, *J* = 2.7 Hz, 1H), 7.59 (dd, *J* = 9.0, 2.7 Hz, 1H), 7.53 (d, *J* = 8.8 Hz, 1H), 7.50 (d, *J* = 2.6 Hz, 1H), 7.12 (d, *J* = 9.0 Hz, 1H), 6.98 (dd, *J* = 8.8, 2.6 Hz, 1H), 3.79 (s, 3H); $^{13}$C NMR (126 MHz, DMSO-$d_6$) δ 158.16, 155.74, 152.69, 148.06, 141.39, 135.86, 132.13, 130.51, 127.12, 119.61 (two non-equivalent carbons), 114.79, 114.45, 105.04, 55.63; HRMS (ESI) calcd for $C_{15}H_{13}N_4O_5S$ $[M+H]^+$ 361.0601, found 361.0595.

**1-(3-Chloro-4-hydroxyphenyl)-3-(6-(dimethylamino)benzo[*d*]thiazol-2-yl)urea (8)**

Beige solid, yield 92 %, m.p. 130 – 132°C; $^1$H NMR (500 MHz, DMSO-$d_6$) δ 10.56 (br s, 1H), 9.89 (s, 1H), 8.98 (s, 1H), 7.60 (d, *J* = 2.6 Hz, 1H), 7.46 (d, *J* = 8.8 Hz, 1H), 7.19 (d, *J* = 2.6 Hz, 1H), 7.17 (dd, *J* = 8.8, 2.6 Hz, 1H), 6.93 (d, *J* = 8.7 Hz, 1H), 6.86 (dd, *J* = 8.9, 2.6 Hz, 1H), 2.91 (s, 6H). $^{13}$C NMR (126 MHz, DMSO-$d_6$) δ 156.08, 152.15, 148.79, 147.47, 139.62, 132.72, 130.92, 120.65, 119.33, 118.04, 116.65, 115.30, 112.69, 103.97, 40.89. HRMS (ESI) calcd for $C_{16}H_{16}ClN_4O_2S$ $[M+H]^+$ 363.0677, found 363.0673.

***N*-(2-(3-(3-Chloro-4-hydroxyphenyl)ureido)benzo[*d*]thiazol-6-yl)acetamide (9)**

Beige solid; yield 71 %; m.p. 190.5 – 191.5°C; $^1$H NMR (500 MHz, DMSO-$d_6$) δ 10.06 (s, 1H), 9.33 (s, 1H), 8.23 (d, *J* = 2.1 Hz, 1H), 7.59 (d, *J* = 2.6 Hz, 1H), 7.56 (d, *J* = 8.7 Hz, 1H), 7.44 (dd, *J* = 8.7, 2.1 Hz, 1H), 7.18 (dd, *J* = 8.8, 2.6 Hz, 1H), 6.94 (d, *J* = 8.7 Hz, 1H), 2.06 (s, 3H); $^{13}$C NMR (126 MHz, DMSO-$d_6$) δ 168.15,

158.61, 152.17, 148.89, 143.73, 134.88, 131.43, 130.82, 120.59, 119.35, 119.26, 119.17, 118.21, 116.70, 111.40, 23.96; HRMS (ESI) calcd for $C_{16}H_{14}ClN_4O_3S$ $[M+H]^+$ 377.0470, found 377.0465.

**Ethyl 2-(3-(3-chloro-4-hydroxyphenyl)ureido)benzo[*d*]thiazole-6-carboxylate (10)**

Beige solid; yield 78 %; m.p. 233 – 234°C; $^1$H NMR (500 MHz, DMSO-$d_6$) δ 11.08 (br s, 1H), 9.95 (s, 1H), 9.04 (s, 1H), 8.54 (s, 1H), 7.96 (dd, *J* = 8.5, 1.8 Hz, 1H), 7.70 (d, *J* = 8.5 Hz, 1H), 7.61 (d, *J* = 2.6 Hz, 1H), 7.20 (dd, *J* = 8.8, 2.6 Hz, 1H), 6.94 (d, *J* = 8.7 Hz, 1H), 4.33 (q, *J* = 7.1 Hz, 2H), 1.34 (t, *J* = 7.1 Hz, 3H); $^{13}$C NMR (126 MHz, DMSO-$d_6$) δ 165.50, 162.93, 151.97, 149.09, 131.39, 130.53, 127.09, 124.14, 123.41, 121.18, 120.92, 119.58, 119.34, 116.64, 60.66, 14.24; HRMS (ESI) calcd for $C_{17}H_{15}ClN_3O_4S$ $[M+H]^+$ 392.0466, found 392.0463.

**2-(3-(3-Chloro-4-hydroxyphenyl)ureido)benzo[*d*]thiazole-6-carboxylic acid (11)**

Ethyl 2-(3-(3-chloro-4-hydroxyphenyl)ureido)benzo[*d*]thiazole-6-carboxylate (**10**) was suspended in a mixture of 1M NaOH and MeOH (1:1) and the reaction mixture was heated at 50°C overnight. After the reaction was completed (monitored by TLC), the reaction mixture was concentrated under reduced pressure and neutralized with 1M HCl. The resulting precipitate was collected by filtration and recrystallized (MeCN) to obtain 2-(3-(3-chloro-4-hydroxyphenyl)ureido) benzo[*d*]thiazole-6-carboxylic acid as a beige solid (0.34 g, 94 %).

Beige solid; yield 94 %; m.p. 265°C (decomp.); $^1$H NMR (500 MHz, DMSO-$d_6$) δ 9.95 (br s, 1H), 9.36 (s, 1H), 8.52 (s, 1H), 7.95 (dd, *J* = 8.4, 1.2 Hz, 1H), 7.68 (d, *J* = 8.4 Hz, 1H), 7.60 (d, *J* = 2.3 Hz, 1H), 7.20 (dd, *J* = 8.7, 2.3 Hz, 1H), 6.95 (d, *J* = 8.7 Hz, 1H); $^{13}$C NMR (126 MHz, DMSO-$d_6$) δ 167.09, 162.63, 152.26, 149.05, 131.23, 130.65, 127.31, 125.08, 123.54, 120.75, 119.41, 119.37, 118.77, 116.71; HRMS (ESI) calcd for $C_{15}H_{11}ClN_3O_4S$ $[M+H]^+$ 364.0153, found 364.0149.

**2-(3-(3-Chloro-4-hydroxyphenyl)ureido)benzo[*d*]thiazole-6-carboxamide (12)**

Beige solid; yield 42 %; m.p. 185 – 186°C; $^1$H NMR (500 MHz, DMSO-$d_6$) δ 9.93 (br s, 1H), 9.25 (s, 1H), 8.42 (d, *J* = 1.8 Hz, 1H), 7.97 (br s, 1H), 7.91 (dd, *J* = 8.4, 1.8 Hz, 1H), 7.66 (d, *J* = 8.4 Hz, 1H), 7.61 (d, *J* = 2.6 Hz, 1H), 7.33 (br s, 1H), 7.20 (dd, *J* = 8.7, 2.6 Hz, 1H), 6.94 (d, *J* = 8.7 Hz, 1H); $^{13}$C NMR (126 MHz, DMSO-$d_6$) δ 167.49, 161.67, 152.34, 150.03, 149.01, 130.86, 130.67, 128.90, 125.71, 121.24, 120.76, 119.43, 119.35, 118.46, 116.68; HRMS (ESI) calcd for $C_{15}H_{12}ClN_4O_3S$ $[M+H]^+$ 363.0313, found 363.0308.

**2-(3-(3-Chloro-4-hydroxyphenyl)ureido)-*N*,*N*-dimethylbenzo[*d*]thiazole-6-carboxamide (13)**

Beige solid; yield 92 %; m.p. 266 – 267°C; $^1$H NMR (500 MHz, DMSO-$d_6$) δ 11.08 (br s, 1H), 9.94 (s, 1H), 9.06 (s, 1H), 7.99 (d, *J* = 1.7 Hz, 1H), 7.65 (d, *J* = 8.3 Hz, 1H), 7.61 (d, *J* = 2.6 Hz, 1H), 7.42 (dd, *J* = 8.3, 1.8 Hz, 1H), 7.20 (dd, *J* = 8.8, 2.6 Hz, 1H), 6.94 (d, *J* = 8.7 Hz, 1H), 2.98 (s, 6H); $^{13}$C NMR (126 MHz, DMSO-

$d_6$) δ 169.87, 161.21, 152.36, 149.01, 148.39, 130.85, 130.79, 130.66, 125.29, 120.84, 119.53, 119.33, 119.33, 118.56, 116.65, 34.99; HRMS (ESI) calcd for $C_{17}H_{16}ClN_4O_3S$ $[M+H]^+$ 391.0626, found 391.0620.

**Procedure D (general conditions): Schiff bases synthesis (14, 16)**

Equimolar amounts of amine and aldehyde were dissolved in toluene (10 mL/mmol) and heated at reflux for 48 h. The solvent was removed under reduced pressure and the crude residue was recrystallized (PE:$Et_2O$) to yield the corresponding product as a yellow solid.

**(*E*)-4-((Benzo[*d*]thiazol-2-ylmethylene)amino)-2-chlorophenol (14)**

Yellow solid; yield 95 %; m.p. 242 – 243°C; $^1$H NMR (500 MHz, DMSO-$d_6$) δ 10.62 (s, 1H), 8.99 (s, 1H), 8.19 – 8.15 (m, 1H), 8.14 – 8.10 (m, 1H), 7.65 (d, *J* = 2.6 Hz, 1H), 7.61 – 7.53 (m, 2H), 7.41 (dd, *J* = 8.6, 2.6 Hz, 1H), 7.06 (d, *J* = 8.6 Hz, 1H); $^{13}$C NMR (126 MHz, DMSO-$d_6$) δ 167.46, 153.55, 153.50, 151.59, 140.62, 134.54, 126.95, 126.78, 123.82, 123.40, 123.10, 122.65, 120.41, 116.82; HRMS (ESI) calcd for $C_{14}H_{10}ClN_2OS$ $[M+H]^+$ 289.0197, found 289.0195.

**(*E*)-2-Chloro-4-(((6-methoxybenzo[*d*]thiazol-2-yl)imino)methyl)phenol (16)**

Yellow solid; yield 84 %; m.p. 260.5 – 261.5°C; $^1$H NMR (500 MHz, DMSO-$d_6$) δ 11.34 (s, 1H), 8.99 (s, 1H), 8.07 (d, *J* = 2.1 Hz, 1H), 7.90 (dd, *J* = 8.5, 2.1 Hz, 1H), 7.80 (d, *J* = 8.8 Hz, 1H), 7.64 (d, *J* = 2.6 Hz, 1H), 7.14 (d, *J* = 8.5 Hz, 1H), 7.10 (dd, *J* = 8.9, 2.6 Hz, 1H), 3.84 (s, 3H); $^{13}$C NMR (126 MHz, DMSO-$d_6$) δ 168.94, 164.36, 157.82, 157.18, 145.55, 135.28, 131.85, 130.29, 127.05, 123.08, 120.64, 117.06, 115.64, 105.09, 55.70; HRMS (ESI) calcd for $C_{15}H_{12}ClN_2O_2S$ $[M+H]^+$ 319.0303, found 319.0302.

**4-((Benzo[*d*]thiazol-2-ylmethyl)amino)-2-chlorophenol (15)**

(*E*)-4-((benzo[*d*]thiazol-2-ylmethylene)amino)-2-chlorophenol (**14**; 1eq) was dissolved in MeOH (10 mL/mmol) and palladium on activated carbon (10% Pd/C; 0.1 eq) was added. The hydrogen atmosphere was introduced and the mixture was stirred at RT overnight [42]. The mixture was filtered through cellite pad and evaporated to dryness. The crude residue was recrystallized ($Et_2O$:EtOH) to obtain 4-((benzo[*d*]thiazol-2-ylmethyl)amino)-2- chlorophenol as a white solid (69 %).

White solid; yield 69 %; m.p. 188.5 – 189.5°C; $^1$H NMR (500 MHz, DMSO-$d_6$) δ 9.10 (s, 1H), 8.02 (d, *J* = 7.8 Hz, 1H), 7.94 (d, *J* = 8.1 Hz, 1H), 7.51 – 7.45 (m, 1H), 7.42 – 7.36 (m, 1H), 6.73 (d, *J* = 8.7 Hz, 1H), 6.62 (d, *J* = 2.8 Hz, 1H), 6.47 (dd, *J* = 8.7, 2.8 Hz, 1H), 6.40 (t, *J* = 6.1 Hz, 1H), 4.62 (d, *J* = 6.1 Hz, 2H); $^{13}$C NMR (126 MHz, DMSO-$d_6$) δ 174.86, 153.13, 144.46, 141.51, 134.53, 125.95, 124.76, 122.25 (two non-equivalent carbons), 120.00, 117.47, 113.54, 112.62, 46.38; HRMS (ESI) calcd for $C_{14}H_{12}ClN_2OS$ $[M+H]^+$ 291.0353, found 291.0349.

**2-Chloro-4-(((6-methoxybenzo[*d*]thiazol-2-yl)amino)methyl)phenol (17)**

(*E*)-2-chloro-4-(((6-methoxybenzo[*d*]thiazol-2-yl)imino)methyl)phenol (**16**; 1 eq) and $NaBH_4$ (1.1 eq) were added to anh. MeOH (10 mL/mmol) and the mixture was stirred at RT overnight. The mixture was diluted with $H_2O$ and extracted with EtOAc (3 × 15 mL), dried over anhydrous $Na_2SO_4$ and the solvent was removed under reduced pressure. The crude residue was recrystallized ($Et_2O$:EtOH) to yield 2-chloro-4-(((6- methoxybenzo[*d*]thiazol-2-yl)amino)methyl)phenol as a white solid (83 %).

White solid; yield 83 %; m.p. 163.5 – 164.5°C; $^1$H NMR (500 MHz, DMSO-$d_6$) δ 10.08 (s, 1H), 8.18 (t, *J* = 5.7 Hz, 1H), 7.33 (d, *J* = 2.1 Hz, 1H), 7.31 (d, *J* = 2.7 Hz, 1H), 7.29 (d, *J* = 8.7 Hz, 1H), 7.14 (dd, *J* = 8.4, 2.2 Hz, 1H), 6.92 (d, *J* = 8.3 Hz, 1H), 6.82 (dd, *J* = 8.7, 2.6 Hz, 1H), 4.43 (d, *J* = 5.4 Hz, 2H), 3.73 (s, 3H); $^{13}$C NMR (126 MHz, DMSO-$d_6$) δ 164.48, 154.36, 152.04, 146.46, 131.40, 130.82, 128.87, 127.30, 119.35, 118.42, 116.48, 112.97, 105.60, 55.54, 46.24; HRMS (ESI) calcd for $C_{15}H_{14}ClN_2O_2S$ $[M+H]^+$ 321.0459, found 321.0454.

**1-(Benzo[*d*]thiazol-2-yl)-*N*-(3-chloro-4-methoxybenzyl)methanamine (37)**

2-(Bromomethyl)benzo[*d*]thiazole (1 eq), (3-chloro-4-methoxyphenyl) methanamine (1.7 eq, 0.51 g) and DIEA (1.7 eq) were dissolved in DCM (10 mL/mmol) and the mixture was stirred at RT for next 24 h. The solvent was removed under reduced pressure and the residue was purified by column chromatography (PE:$CHCl_3$, 1:1) to yield 1-(benzo[*d*]thiazol-2-yl)-*N*-(3-chloro-4-methoxybenzyl)methanamine as a light yellow oil (96 %).

$^1$H NMR (500 MHz, Chloroform-*d*) δ 7.99 – 7.95 (m, 1H), 7.91 – 7.87 (m, 1H), 7.49 – 7.44 (m, 1H), 7.42 (d, *J* = 2.1 Hz, 1H), 7.40 – 7.35 (m, 1H), 7.23 (dd, *J* = 8.4, 2.1 Hz, 1H), 6.90 (d, *J* = 8.4 Hz, 1H), 4.23 (s, 2H), 3.90 (s, 3H), 3.84 (s, 2H).

**4-(((Benzo[*d*]thiazol-2-ylmethyl)amino)methyl)-2-chlorophenol (18)**

1-(Benzo[*d*]thiazol-2-yl)-*N*-(3-chloro-4-methoxybenzyl)methanamine (**37**; 1 eq) was dissolved in anhydrous DCE (6 mL/mmol) and nitrogen atmosphere was introduced. Aluminium chloride (3 eq) was added portion-wise and the mixture was heated at 60°C overnight. The reaction mixture was cooled down to RT, quenched with $H_2O$, partitioned between $H_2O$:EtOAc and extracted with EtOAc (3 × 25 mL). The organic layers were combined, dried over anhydrous $Na_2SO_4$ and the solvent was removed under reduced pressure. The residue was purified by column chromatography (PE:EtOAc, 2:1) to yield 4-(((benzo[*d*]thiazol-2-ylmethyl)amino)methyl)- 2-chlorophenol as a white solid (45 %).

White solid; yield 45 %; m.p. 120 – 121°C; $^1$H NMR (500 MHz, Chloroform-*d*) δ 8.00 – 7.95 (m, 1H), 7.90 – 7.86 (m, 1H), 7.49 – 7.44 (m, 1H), 7.40 – 7.36 (m, 1H), 7.35 (d, *J* = 2.1 Hz, 1H), 7.13 (dd, *J* = 8.3, 2.1 Hz, 1H), 6.94 (d, *J* = 8.3 Hz, 1H), 4.23 (s, 2H), 3.82 (s, 2H); $^{13}$C NMR (126 MHz, Chloroform-*d*) δ 173.26,

153.36, 150.94, 135.10, 132.71, 129.03, 128.39, 126.14, 125.06, 122.83, 121.91, 120.18, 116.43, 52.38, 50.68; HRMS (ESI) calcd for $C_{15}H_{14}ClN_2OS$ $[M+H]^+$ 305.0510, found 305.0508.

**2-(Chloromethyl)benzo[*d*]oxazole (39)**

2-aminophenol (1 eq) and chloroacetyl chloride (1.5 eq) were dissolved in *o*-xylene (6 mL/mmol) under nitrogen atmosphere. TEA (1.1 eq) was added dropwise and the reaction mixture was stirred at 145°C overnight. The mixture was diluted with 20 mL sat. aq. $NH_4Cl$ and extracted with EtOAc (3 × 6 mL), The organic phase was dried over anhydrous $Na_2SO_4$ and solvents were removed under reduced pressure. The residue was purified by column chromatography (PE:EtOAc, 6:1) to yield 2-(chloromethyl)benzo[*d*]oxazole as a yellow oil (71 %).

$^1$H NMR (500 MHz, DMSO-$d_6$) δ 7.78 (t, *J* = 7.4 Hz, 2H), 7.51 – 7.37 (m, 2H), 5.08 (s, 2H).

**1-(Benzo[*d*]oxazol-2-yl)-*N*-(3-chloro-4-methoxybenzyl)methanamine (40)**

2-(Chloromethyl)benzo[*d*]oxazole (**39**; 1 eq), (3-chloro-4-methoxyphenyl)methanamine (1.5 eq) and DIEA (2 eq) were dissolved in anh. MeCN (8 mL/mmol) under nitrogen atmosphere. The reaction mixture was stirred at 70°C overnight. The reaction mixture was concentrated at reduced pressure. The crude residue was purified by column chromatography ($CHCl_3$:MeOH, 100:1) to yield 1-(benzo[*d*]oxazol-2-yl)-*N*-(3-chloro-4-methoxybenzyl)methanamine as a yellow oil (79 %).

$^1$H NMR (500 MHz, DMSO-$d_6$) δ 7.76 – 7.63 (m, 2H), 7.44 – 7.30 (m, 3H), 7.25 (dd, *J* = 8.4, 2.1 Hz, 1H), 7.06 (d, *J* = 8.4 Hz, 1H), 3.94 (s, 2H), 3.81 (s, 3H), 3.72 (s, 2H), 3.00 (br s, 1H).

**4-(((Benzo[*d*]oxazol-2-ylmethyl)amino)methyl)-2-chlorophenol (19)**

1-(Benzo[*d*]oxazol-2-yl)-*N*-(3-chloro-4-methoxybenzyl)methanamine (**40**; 1 eq) was dissolved in anh. DCE (10 mL/mmol) under nitrogen atmosphere, aluminium trichloride (3.5 eq) was added and the reaction mixture was stirred at 60°C overnight. The reaction mixture was concentrated at reduced pressure. The residue was diluted with $H_2O$, pH was adjusted to 7 using sat. aq. $NaHCO_3$ solution. The product was extracted with EtOAc (3 × 10 mL), dried over anhydrous $Na_2SO_4$ and the solvent was removed under reduced pressure. The crude residue was purified by column chromatography ($CHCl_3$:MeOH, 30:1). Resulting oily compound was recrystallized from PE to yield 4-(((benzo[*d*]oxazol-2-ylmethyl)amino)methyl)-2-chlorophenol as white solid (46 %).

White solid; yield 46 %; m.p. 99 – 100.5 °C; $^1$H NMR (500 MHz, Chloroform-*d*) δ 7.74 – 7.69 (m, 1H), 7.54 – 7.49 (m, 1H), 7.36 – 7.31 (m, 3H), 7.12 (dd, *J* = 8.3, 2.0 Hz, 1H), 6.92 (d, *J* = 8.3 Hz, 1H), 4.08 (s, 2H), 3.81 (s, 2H); $^{13}$C NMR (126 MHz, Chloroform-*d*) δ 165.08, 150.97, 150.93, 140.97, 132.37, 129.16,

128.47, 125.18, 124.57, 120.20, 120.03, 116.47, 110.75, 52.19, 45.70; HRMS (ESI) calcd for $C_{15}H_{14}ClN_2O_2$ $[M+H]^+$ 289.0738, found 289.0733.

***N*-((1*H*-indol-2-yl)methyl)-1-(3-chloro-4-methoxyphenyl)methanamine (41)**

1*H*-indole-2-carbaldehyde (1 eq) was dissolved in anh. MeOH (7 mL/mmol) under nitrogen atmosphere and the solution was cooled to 0°C. (3-chloro-4-methoxyphenyl)methanamine (1 eq) was dissolved in anh. MeOH (1 mL/mmol) and was added dropwise to the reaction mixture at 0°C. The reaction was warmed up to RT and stirred overnight. Then the reaction mixture was cooled to 0°C and $NaBH_3CN$ (1.5 eq) was added. The reaction mixture was stirred at RT overnight. The solvent was evaporated and the residue was diluted with $H_2O$. The product was extracted with EtOAc (3 × 10 mL), dried over anhydrous $Na_2SO_4$ and the solvent was removed under reduced pressure. The crude residue was purified by column chromatography ($CHCl_3$ mobile phase) to yield *N*-((1*H*-indol-2-yl)methyl)-1-(3-chloro-4-methoxyphenyl)methanamine as a yellow oil (43 %).

$^1$H NMR (300 MHz, DMSO-$d_6$) δ 10.93 (br s, 1H), 7.48 – 7.39 (m, 2H), 7.35 – 7.29 (m, 1H), 7.26 (dd, *J* = 8.4, 2.1 Hz, 1H), 7.08 (d, *J* = 8.5 Hz, 1H), 7.04 – 6.96 (m, 1H), 6.96 – 6.88 (m, 1H), 6.25 (d, *J* = 1.1 Hz, 1H), 3.83 (s, 3H), 3.78 (s, 2H), 3.64 (s, 2H), 2.63 (br s, 1H).

**4-((((1*H*-indol-2-yl)methyl)amino)methyl)-2-chlorophenol (20)**

*N*-((1*H*-indol-2-yl)methyl)-1-(3-chloro-4-methoxyphenyl)methanamine (**41**; 1 eq) was dissolved in anh. DCE (12 mL/mmol) under nitrogen atmosphere, aluminium trichloride (3.5 eq) was added and the reaction mixture was stirred at 60°C for 7h. The reaction mixture was concentrated at reduced pressure. The residue was diluted with $H_2O$ and the product was extracted with EtOAc (3 × 10 mL), dried over anhydrous $Na_2SO_4$ and the solvent was removed under reduced pressure. The crude residue was purified by column chromatography ($CHCl_3$:MeOH, 20:1 + 1% TEA) to yield 4-((((1*H*-indol-2-yl)methyl)amino)methyl)-2-chlorophenol as a light-beige solid (30 %).

Light-beige solid; yield 30 %; m.p. 136 – 138 °C; $^1$H NMR (500 MHz, DMSO-$d_6$) δ 10.92 (s, 1H), 7.43 (d, *J* = 7.8 Hz, 1H), 7.37 – 7.28 (m, 2H), 7.09 (dd, *J* = 8.3, 2.0 Hz, 1H), 7.04 – 6.98 (m, 1H), 6.96 – 6.88 (m, 2H), 6.25 (d, *J* = 1.1 Hz, 2H), 3.78 (s, 2H), 3.60 (s, 2H); $^{13}$C NMR (126 MHz, DMSO-$d_6$) δ 151.66, 138.79, 136.12, 132.44, 129.25, 128.01, 127.68, 120.29, 119.37, 119.31, 118.57, 116.26, 110.91, 99.15, 51.08, 45.37; HRMS (ESI) calcd for $C_{16}H_{16}ClN_2O$ $[M+H]^+$ 287.0946, found 287.0945.

### 4.3 Log*P* and Log*D* Determination

The distribution coefficient of prepared compounds between water – octanol (log*P*) and PBS buffer of pH 7.4 – octanol (log*D*) was determined by UHPLC-DAD-MS measurement of analyte concentration in

particular solvent using Agilent 1290 Infinity II chromatography system coupled with Agilent 6470 OqQ mass spectrometer (Agilent Technologies, Santa Clara, USA). Compounds were weighed (0.25 mg) and dissolved in 500 µL of water/buffer – octanol mixture (1:1 (v/v) ratio). Samples were shaken for 30 min and subsequently centrifuged for 10 min at 10,000 rcf. Aqueous and octanol phases were transferred into vials and analysed. The concentration of analyte in a particular phase was determined according to an adequate calibration line.

### 4.4 p$K_a$ Determination

The negative decimal logarithms of the dissociation constants (p$K_a$) of prepared compounds were determined spectrophotometrically using buffers of given pH (range from 3.0 to 11.5 with 0.5 unit increment). Ten microliters of tested compound (1 mg/mL) were dissolved in 490 µL of particular buffer and absorbance spectra of various dissociation states were scanned in the range 200-400 nm using Carry-60 UV-VIS spectrophotometer (Agilent Technologies, Santa Clara, USA) at 20 °C. The p$K_a$ values were calculated from the sigmoidal dependence of the absorbance of the dissociated form of the substance on the pH value using GraphPad Prism 8.2 software (San Diego, USA).

### 4.5 Solubility

Compound solubility determination was performed using nephelometry assays on NEPHELOstar microplate instrument (BMG Labtech, Offenburg, Germany). Stock solutions of analyzed compounds were prepared in a concentration 160 µg/mL in phosphate buffer (pH = 7.4). Each suspension was sonicated at full power with Hielscher UP100H needle ultrasonic processor (Teltow, Germany) to achieve uniform dispersion of particles. Immediately after sonication, the suspension was loaded into NEPHELOstar instrument injector A, together with phosphate buffer (pH = 7.4) loaded into injector B. Compound dilution was then performed automatically in 48 wells in range 0 to 160 µg/mL. After 30 seconds of shaking, each well was scanned with 80% laser power in matrix 3×3, beam width 2 mm. If necessary, the process was repeated with a higher concentration of stock solution (640 ug/mL and 2.54 mg/mL). Obtained data were evaluated in Graphpad Prism 7.03 using segmental linear regression.

### 4.6 Enzyme Inhibition

The recombinant 17β-HSD10 was expressed in *Escherichia coli* BL21 (DE3) strain and purified as described previously [22]. For the compounds' inhibitory potency and $IC_{50}$ determination, the SAAC method using acetoacetyl-CoA (AAC) as a substrate and absorbance readout at 340 nm was used [22]. In brief, 0.15 µg of recombinant 17β-HSD10 was mixed with 320 µmol/L nicotinamide adenine dinucleotide (NADH) as an enzyme cofactor in assay buffer (10 mM Tris-HCl, pH 7.4, 150 mM NaCl, 1 mM dithiothreitol (DTT), 0.001 % Tween 20 and 0.01 % bovine serum albumin) and the mixture was

preincubated for 5 minutes at 37 °C with the tested inhibitor (or vehicle control). The reaction was started by the addition of 320 µmol/L AAC and monitored as a change in absorbance at 340 nm for 5 minutes in 10-sec intervals. Inhibitors were dissolved in anhydrous DMSO and further diluted in DMSO and assay buffer to reach the final inhibitor concentrations. All data were analysed in GraphPad Prism 7 software using non-linear regression, and $IC_{50}$ values were calculated for each inhibitor from at least three independent measurements, all in triplicate. The data are expressed as the mean ± SD.

### 4.7 Molecular docking

For the purposes of molecular docking, two crystal structures of 17β-HSD10 (PDB ID: 1U7T with resolution 2.00 Å and PDB ID: 1E6W with resolution 1.70 Å) were obtained from the online PDB database (www.rcsb.org). The ligands under investigation were generated by Avogadro v1.2.0 [43] and consequently geometrically optimized using MMFF94 force field. Two docking methods, AutoDock: Vina v1.1.3 [27] and MOE v2022.02 [28] respectively, were employed in the molecular docking experiment.

Following procedure was adopted to conduct the flexible docking in AD: Vina: UCSF Chimera v1.16 [44] was used for the initial process of removal of the surplus copies of the enzyme chains, non-bonded inhibitors and other small molecules (except for NAD). AutoDockFR suite v1.0 [45] and OpenBabel library v2.4.1 [46] were used to add hydrogen atoms and to assign the partial charges to all atoms in both enzymes. Residues Ser155, Tyr168 and Lys172 from the active site were selected as flexible. The rotatable bonds in the flexible residues were detected automatically by AutoDock Tools v1.5.4. Centre of the grid box was selected as the centre of an estrone molecule that was co-crystallized with 1E6W, or center of the cavity in the active site of 1U7T respectively. Size of x, y, and z sides of the grid box was set to 25 Å. AD: Vina docking was then performed using exhaustiveness parameter of 32, employing 12 CPUs in parallel multithreading. 10 replicate dockings were conducted for every ligand. Resulting complexes with minimal predicted Gibbs binding energy were selected as the top-scoring.

In MOE, the initial process of removal of the surplus copies of the enzyme chains, non-bonded inhibitors and other small molecules (except for NAD) was followed by receptor preparation using MOE-QuickPrep, which included addition of hydrogen atoms and assigning the partial charges to all atoms in both enzymes. Ligand placement was performed using the Triangle Matcher protocol, which defines the active site using α-spheres, that were generated using the MOE-SiteFinder application. The top 1,000 poses produced from placement were then scored using the London dG scoring function. The top 30 poses as ranked by London dG were kept and minimized using MMFF94x within a flexible receptor. The resulting poses were then scored using the GBVI/WSA dG scoring function.

Superpositions of selected top-scoring ligands were visualised by VMD v1.9.4 [47] and edited in GIMP v2.10 (www.gimp.org).

### 4.8 Mitochondrial assays

#### *4.8.1 Pig Brain Mitochondria*

A crude mitochondrial fraction was isolated from the brain cortex of slaughtered pigs by the standard differential centrifugation technique. Purified mitochondria were separated from the crude mitochondrial fraction by centrifugation with a sucrose gradient and used for the assays [48]. A cytochrome *c* test was used to evaluate the intactness of the outer mitochondrial membrane in mitochondrial preparations. Damage to the inner mitochondrial membrane was assessed by measuring the release of the matrix enzyme citrate synthase (CS). Mitochondria were stored in a preservation medium on the ice at a total protein concentration of 20–50 mg/mL. The concentration of proteins was determined by the Lowry method [49] with bovine serum albumin as a standard.

#### *4.8.2 Citrate Synthase and Complex I and Complex II+III Activity*

The activity of CS (E.C. 2.3.3.1) and mitochondrial Complex I (E.C. 7.1.1.2) and the couple Complex II (E.C. 1.3.5.1) and III (E.C. 7.1.1.8) was measured spectrophotometrically using an Uvikon XL spectrophotometer (Secomam, Ales, France). Isolated pig brain mitochondria were diluted in hypotonic buffer (25 mM potassium phosphate and 5 mM $MgCl_2$, pH 7.2) and shortly ultrasonicated three times to stimulate the enzyme to the highest activity. The drug was incubated with mitochondria at 30 °C for 30 min. The drug-free solvent (DMSO) was added to the control sample. The total sample volume was 1 mL; the measurement temperature was 30 °C.

CS activity was measured as the color change of 5,5'-dithiobis-(2-nitrobenzoic acid) (DTNB) according to a method published by Srere [29]. The incubation medium was composed of 0.2 mM DTNB, 0.1 mM acetyl-CoA, 0.1 % Triton X-100, 100 mM Tris/HCl (pH 8.1), mitochondria (20 µg/mL mitochondrial protein), and 50 µM of drug. The reaction was initiated by adding the oxaloacetate (0.5 mM) and measured at 412 nm for 3 min.

The activity of respiratory Complex I was measured based on the rotenone-sensitive rate of the NADH oxidation; a slightly modified previously published method [30] was used. The incubation medium was composed of phosphate buffer (25 mM $KH_2PO_4$, 5 mM $MgCl_2$, pH 7.2), 2 mM KCN, mitochondria (1 mg/mL of mitochondrial protein), and 50 µM drug. The reaction was initiated by coenzyme $Q_{10}$ (100 µM) and NADH (100 µM) and measured at 340 nm for 5 min. A background correction was verified, which was measured under the same conditions after inhibition of the Complex I by 10 µM rotenone.

The couple Complex II + III activity was determined as the rate of reduction of cytochrome *c* measured at 550 nm for 3 min [32,50]. The final mitochondrial protein concentration was 0.5 mg/ml. The medium contained 50 mM $KH_2PO_4$, 0.625 mM EDTA, 20 mM succinate, 0.1 mM rotenone (Complex I inhibitor that ensured that cytochrome *c* reduction occurs via Complex II), 2 mM KCN (cytochrome *c* oxidase inhibitor that prevented the re-oxidation of cytochrome *c*), and 50 µM drug. The reaction is started by the addition of 30 µmol/L cytochrome *c*.

#### *4.8.3 Mitochondrial Respiration*

*In vitro* effects of the test compounds on electron transport system activity were measured by high-resolution respirometry as drug-induced changes in the rate of oxygen consumption in isolated mitochondria in state 3 respiration, as previously described [33,48]. The Oxygraph-2k equipped with two tempered chambers and Clark-type electrodes and an automatic titration-injection micropump TIP2k (Oroboros Instruments, Innsbruck, Austria) was used [51]. Briefly, following substrate addition was made (malate + pyruvate + ADP for Complex I-linked respiration and ADP + rotenone + succinate for Complex II-linked respiration), the sample was titrated with a drug in one chamber and with DMSO in the second chamber. Drug-induced changes in oxygen flow were determined with 10–20 different drug concentrations (the final concentrations were set within the range of 1.25–500 µM).

#### *4.8.4 Monoamine Oxidase Assay*

The activities of MAO-A and MAO-B were assayed using radiochemical method by the modification of a previously published experimental protocol [34] with either tritium-labelled serotonin ([$^3$H]5-HT) as the MAO-A substrate and $^{14}$C-labelled phenylethylamine ([$^{14}$C]PEA) as the MAO-B substrate. The reaction mixture containing the mitochondria and a drug at 5–7 various concentrations (final drug concentrations ranged from 1 µM to 1000 µM) was preincubated at 37 °C for 60 min. The reaction was initiated by the addition of the radiolabelled substrate and terminated after 20 min (MAO-A activity) or 1 min (MAO-B activity) incubation. The MAO activities were determined by measuring the radioactivity levels of the corresponding aldehyde, resulting from oxidative deamination of [$^3$H]5-HT or [$^{14}$C]PEA, using an LS 6100IC liquid scintillation counter (Beckman Instruments, Inc., Fullerton, CA, USA).

#### *4.8.5 Data Analysis*

DatLab software (Oroboros Instruments, Innsbruck, Austria) was used for respirometry data acquisition and analysis. To correct for a slight decrease in respiratory rate during experiments lasting more than 1 h, the relative respiratory rate was calculated as the ratio of the oxygen consumption rate

in the sample titrated with a drug to the oxygen consumption rate in the sample titrated with the solvent (DMSO).

Plotted dose-response curves of the activity were analysed by four-parameter logistic regression using SigmaPlot software (Inpixon HQ, Palo Alto, CA 94303, USA), and the half-maximal inhibitory concentration ($IC_{50}$) was established, which represents the drug concentration required to inhibit by 50 % the difference between baseline (no drug) and residual value (drug overdose) of mitochondrial respiratory rate or MAO activity.

Statistical analyses were performed using a Statistica data analysis software system (TIBCO Software Inc., Palo Alto, CA, USA). Data are presented as the mean ± standard error (SE) or the mean ± standard deviation (SD).

### 4.9 CellTox Green Cytotoxicity Assay and CellTiter-Glo Cell Viability Assay

HEK293 and SH-SY5Y cells were maintained in DMEM (Capricorn) supplemented with 10 % fetal bovine serum (Gibco), 2 mM L-glutamine (Lonza) and non-essential amino acids additives (Gibco) at 37 °C, under a humidified atmosphere of 5% $CO_2$. Selected compounds (**6**, **9**, **11**, **12**) were tested on HEK293 and SH-SY5Y cell lines to determine their cytotoxic effects and impact on cell viability using CellTox Green and CellTiter-Glo 2.0 kits (Promega G8741 and G9241, respectively), respectively. The measurements were performed as endpoint methods in the multiplex using a TECAN SPARK® instrument. For multiplex measurement, 7,500 cells were seeded per well in 50 µL of culture media and cultured for 24 h before adding selected compounds. The compounds were dissolved in anhydrous DMSO, further diluted in DMSO and added to the wells at a final compound concentration of 1 µM and 10 µM (1% DMSO concentration). The cells treated with 1% DMSO only were used as a vehicle control and 100 µM valinomycin treatment was used as a positive control. After the treatment, the cells were cultured for additional 48 h followed by the multiplex measurement. The measurements were performed in a white solid bottom 96 well microplates (Grainer Bio-One 655083) following the manufacturer's protocol. The fluorescent CellTox Green Cytotoxicity Assay was measured first (ex 485 nm and em 530 nm wavelengths) followed by the the CellTiter-Glo Luminescent Cell Viability Assay with an integration time of 500 ms.

### 4.10 Dehydrogenase Activity and Glutathione Assay

SH-SY5Y cells (ATCC CRL-2266), a human neuroblastoma cell line, was cultured in Dulbecco's Modified Eagle's Medium/Nutrient Mixture F-12 w/wo phenol red supplemented with 15% (v/v) fetal bovine serum, 50 µg/mL penicillin, 50 µg/mL streptomycin, 1% (v/v) nonessential amino acids and 2 mM glutamine and maintained at 37 °C in a sterile, humidified atmosphere of 5% $CO_2$. All the experiments

were conducted using SH-SY5Y cells in passages 14–18. The cells were cultured for 4 and 24 h with selected compounds.

Glutathione (GSH) levels were measured using the optimized monochlorobimane spectrofluorometric assay [52]. After cell treatment, 20 µL of the bimane solution was added to cells to obtain the final concentration 40 µmol/L and the spectrofluorometric measurement was started immediately. The fluorescence increase (EX/EM = 394/490 nm) was measured for 10 min using a Tecan Spark fluorescence microplate reader (Tecan, Switzerland). The fluorescence was expressed as the slope of change in fluorescence over time. The glutathione levels were expressed as the percentage relative to the glutathione levels in control cells (= 100%). The results were expressed as mean ± SD.

Dehydrogenase activity was assessed by WST-1 test (Roche, Germany). The WST-1 test measures the activity of intra- and extramitochondrial dehydrogenases. After cell treatment, 10 µL of WST-1 reagent was added to the cultured cells. The absorbance change (0–1 h) was measured spectrophotometrically at wavelength of 440 nm using a Tecan Spark fluorescence microplate reader (Tecan, Switzerland). The cell viability was expressed as the percentage of intra- and extramitochondrial dehydrogenases activity relative to that in control cells (= 100%). The results were expressed as mean ± SD. The maximal background absorbance was lower than 15% of a signal in untreated cells.

### 4.11 Thermal Shift Assay

Melting temperatures ($T_m$) were measured in 100 mM potassium phosphate buffer (pH 8.0) containing a 1:1000 dilution of SYPRO Orange (Sigma-Aldrich) and 1.43 µM 17β-HSD10. The compounds were tested at two concentrations (25 and 50 µmol/L) in the total reaction volume of 40 µL. The fluorescence melting curve was monitored in a temperature range from 25 to 90 °C in the temperature ramps of 1 °C/min using qTOWER³ real-time PCR thermal cycler (Analytic Jena; Ex/Em = 490/575). Melting curves were analysed and melting temperatures were determined using qPCRsoft 4.0. All measurements were performed in triplicate.

### 4.12 Parallel Artificial Membrane Permeability Assay (PAMPA–BBB)

The filter membrane of the donor plate was coated with PBL (Polar Brain Lipid, Avanti, AL, USA) in dodecane (4 µL of 20 mg/mL PBL in dodecane) and the acceptor well was filled with 300 µL of PBS pH 7.4 buffer ($V_A$). Tested compounds were dissolved first in DMSO and that diluted with PBS pH 7.4 to reach the final concentration in the range between 25–100 µM in the donor well. The concentration of DMSO did not exceed 0.5% (*v*/*v*) in the donor solution. 300 µL of the donor solution was added to the donor wells ($V_D$) and the donor filter plate was carefully put on the acceptor plate so that coated membrane was “in touch” with both donor solution and acceptor buffer. Test compound diffused from

the donor well through the lipid membrane (Area = 0.28 $cm^2$) to the acceptor well. The concentration of the drug in both donor and the acceptor wells were assessed after 3, 4, 5 and 6 h of incubation in quadruplicate using the UV plate reader Synergy HT (Biotek, Winooski, VT, USA) at the maximum absorption wavelength of each compound. Besides that, the solution of theoretical compound concentration, simulating the equilibrium state established if the membrane were ideally permeable was prepared and assessed as well. The concentration of the compounds in the donor and acceptor well and equilibrium concentration were calculated from the standard curve and expressed as the permeability (Pe) according to the equation:

$$\log Pe = \log\left\{C \times -\ln\left(1 - \frac{[drug]_{acceptor}}{[drug]_{equilibrium}}\right)\right\} \quad \text{where } C = \left(\frac{V_D \times V_A}{(V_D + V_A) \times Area \times Time}\right)$$

### 4.13 *In Vivo* Experiments

#### *4.13.1 Animals*

Male albino Wistar rats weighing 220–250 g were purchased from Velaz (Prague, Czech Republic). They were kept in an air-conditioned enclosure with light from 07:00 *a.m.* to 7:00 *p.m.* and were allowed access to standard food and tap water *ad libitum*. During the housing, rats were divided into groups of 6 animals. The pharmacokinetic study was performed following ethical guidelines. The handling of the experimental animals was performed under the supervision of the Ethics Committee of the Faculty of Military Health Sciences, Czech Republic (No. MO 103046/2018-684800, and MO 268874/2018-684800).

#### *4.13.2 Pharmacokinetic Study*

After intravenous (i.v.) administration of **9** (15.06 µg/kg; 0.2 mL/100 g *b.w.*, *3 % DMSO in saline*) and **11** (18.18 µg/kg; 0.2 mL/100 g *b.w.*, *3 % DMSO in saline*) blood samples were collected from the rats under deep terminal anaesthesia ($CO_2$) by cardiac puncture and stored in heparinised 1.5 mL tubes at 0, 5, 15, 30, 60, 90, 180, 240, 360 and 1440 min (*n = 3*). After oral administration of **9** and **11** (both 60 mg/kg; 1 mL/100 g *b.w.*, *25 % Kolliphor + 10 % NMP in saline*) blood samples were collected in the same way at 0, 5, 15, 30, 45, 60, 120, 180, 240, 300, 360, 420, 480, 540, 600 and 1440 min (*n = 3*). All blood samples were immediately centrifuged at 3000 × *g* for 10 min (10 °C), and the plasma was divided into two parts.

As the blood in organ vessels also contained the studied molecules, this would have interfered with the accuracy of the brain concentration assay. Therefore, the animals were perfused transcardially with saline solution (0.9% NaCl) for 5 min (10 mL/min). After perfusion, the skull was opened, and the brain was carefully removed. Brains were stored at -80 °C until analysis.

*4.13.3 Sample Analysis*

Frozen brains were homogenized in cold PBS (w/v 1:4) using Fastprep-24 5G sample disruption instrument. Thawed plasma or homogenized brain in the volume of 100 µL, was mixed with the same volume of methanol and acetonitrile, vortexed for 15 minutes and centrifuged at 14000 g for 3 minutes. The supernatant was then filtered through 0.22 µm PTFE syringe filter into the vial and measured.

Detection of **9** and **11** was performed on the Agilent 1290 Infinity II UHPLC system coupled to the Agilent 6470 QqQ mass spectrometer. Chromatographic conditions were maintained at gradient elution of 0.4 mL/min by 0.1% formic acid in water and acetonitrile (0-0.5 70:30, 0.5-3.0 gradient to 10:90, 3.0-3.6 10:90, 3.6-5.0 70:30), thermostated autosampler set to 15 °C and column thermostat equipped with the Zorbax Eclipse plus RRHD C18 2.1×50 mm, 1.8 µm (PN 959757-902) column kept to 25 °C. MS source parameters for detection of compound **9** were set to the following: drying gas 320 °C at 4 L/min, sheath gas 400 °C at 12 L/min, nebulizer pressure 35 psi, capillary voltage 3500 V and nozzle voltage 300 V. Transitions of $[M+H]^+$ ions m/z were detected with setting of dwell time 200 ms, cell accelerator 4 V, fragmentor 129 V for 377→208, 166 and 133 (CE 24, 44 and 60 V). MS source parameters for detection of compound **11** were set to the following: drying gas 260 °C at 12 L/min, sheath gas 400 °C at 12 L/min, nebulizer pressure 30 psi, capillary voltage 3500 V and nozzle voltage 900 V. Transitions of $[M+H]^+$ ions m/z were detected with setting of dwell time 200 ms, cell accelerator 4 V, fragmentor 129 V for 364→195, 151 and 109 (CE 20, 48 and 60 V).

*4.13.4 Data Evaluation*

Standard non-compartmental analysis was performed using the Kinetica software, version 4.0 (InnaPhase Corporation, Thermo Fisher Scientific Inc., Waltham, MA, USA). The maximum concentration ($C_{max}$) and the time to the maximum concentration ($T_{max}$) were determined directly from the observed data. The area under the mean plasma concentration-time curve from zero to 1440 min ($AUC_{0\text{-}1440min}$) was defined. The $\lambda_z$ (terminal rate constant) was estimated using linear regression of the log-transformed concentrations plotted against time. The half-life was calculated as follows: $t_{1/2} = ln(2)/\lambda_z$.

**Acknowledgement**

This study was supported by the Ministry of Education, Youth, and Sports of the Czech Republic (project ESF no. CZ.02.1.01/0.0/0.0/18_069/0010054), by the University of Hradec Kralove (Faculty of Science, no. SV2103-2022), by Charles University, Prague, Czech Republic (project Cooperatio, research area Neurosciences), by the project MH CZ-DRO VFN64165, and by MH CZ - DRO (UHHK, 00179906), by the Ministry of Defence of the Czech Republic (Faculty of Military Health Sciences Hradec Kralove) under the grant entitled the "Long-term organization development plan - Medical Aspects of Weapons of Mass Destruction", and by the RS MacDonald Charitable Trust and Rosetrees Trust.

**References**

[1] L. Vinklarova, M. Schmidt, O. Benek, K. Kuca, F. Gunn-Moore, K. Musilek, Friend or enemy? Review of 17β-HSD10 and its role in human health or disease, Journal of Neurochemistry. 155 (2020) 231–249. https://doi.org/10.1111/jnc.15027.

[2] Z. Fišar, Linking the Amyloid, Tau, and Mitochondrial Hypotheses of Alzheimer's Disease and Identifying Promising Drug Targets, Biomolecules. 12 (2022) 1676. https://doi.org/10.3390/biom12111676.

[3] H. Hampel, J. Hardy, K. Blennow, C. Chen, G. Perry, S.H. Kim, V.L. Villemagne, P. Aisen, M. Vendruscolo, T. Iwatsubo, C.L. Masters, M. Cho, L. Lannfelt, J.L. Cummings, A. Vergallo, The Amyloid-β Pathway in Alzheimer's Disease, Mol Psychiatry. 26 (2021) 5481–5503. https://doi.org/10.1038/s41380-021-01249-0.

[4] A. Morsy, P.C. Trippier, Amyloid-Binding Alcohol Dehydrogenase (ABAD) Inhibitors for the Treatment of Alzheimer's Disease, Journal of Medicinal Chemistry. 62 (2018) 4252–4264. https://doi.org/10.1021/acs.jmedchem.8b01530.

[5] O. Benek, L. Aitken, L. Hroch, K. Kuca, F. Gunn-Moore, K. Musilek, A Direct Interaction Between Mitochondrial Proteins and Amyloid-beta Peptide and its Significance for the Progression and Treatment of Alzheimer's Disease, Curr. Med. Chem. 22 (2015) 1056–1085. https://doi.org/10.2174/0929867322666150114163051.

[6] X.-Y. He, S.-Y. Yang, Roles of Type 10 17beta-Hydroxysteroid Dehydrogenase in Intracrinology and Metabolism of Isoleucine and Fatty Acids, Endocrine, Metabolic & Immune Disorders - Drug Targets. 6 (2006) 95–102. https://doi.org/10.2174/187153006776056639.

[7] D. Ayan, R. Maltais, D. Poirier, Identification of a 17β-Hydroxysteroid Dehydrogenase Type 10 Steroidal Inhibitor: A Tool to Investigate the Role of Type 10 in Alzheimer's Disease and Prostate Cancer, ChemMedChem. 7 (2012) 1181–1184. https://doi.org/10.1002/cmdc.201200129.

[8] X.-Y. He, Y.-Z. Yang, D.M. Peehl, A. Lauderdale, H. Schulz, S.-Y. Yang, Oxidative 3α-hydroxysteroid dehydrogenase activity of human type 10 17β-hydroxysteroid dehydrogenase, The Journal of Steroid Biochemistry and Molecular Biology. 87 (2003) 191–198. https://doi.org/10.1016/j.jsbmb.2003.07.007.

[9] E.A. Carlson, R.T. Marquez, F. Du, Y. Wang, L. Xu, S.S. Yan, Overexpression of 17β-hydroxysteroid dehydrogenase type 10 increases pheochromocytoma cell growth and resistance to cell death, BMC Cancer. 15 (2015) 166. https://doi.org/10.1186/s12885-015-1173-5.

[10] C.R. Kissinger, P.A. Rejto, L.A. Pelletier, J.A. Thomson, R.E. Showalter, M.A. Abreo, C.S. Agree, S. Margosiak, J.J. Meng, R.M. Aust, D. Vanderpool, B. Li, A. Tempczyk-Russell, J.E. Villafranca,

Crystal Structure of Human ABAD/HSD10 with a Bound Inhibitor: Implications for Design of Alzheimer's Disease Therapeutics, Journal of Molecular Biology. 342 (2004) 943–952. https://doi.org/10.1016/j.jmb.2004.07.071.

[11] A. Morsy, K. Maddeboina, J. Gao, H. Wang, J. Valdez, L.F. Dow, X. Wang, P.C. Trippier, Functionalized Allopurinols Targeting Amyloid-Binding Alcohol Dehydrogenase Rescue Aβ-Induced Mitochondrial Dysfunction, ACS Chem. Neurosci. 13 (2022) 2176–2190. https://doi.org/10.1021/acschemneuro.2c00246.

[12] S. Boutin, J. Roy, R. Maltais, W. Alata, F. Calon, D. Poirier, Identification of steroidal derivatives inhibiting the transformations of allopregnanolone and estradiol by 17β-hydroxysteroid dehydrogenase type 10, Bioorganic & Medicinal Chemistry Letters. 28 (2018) 3554–3559. https://doi.org/10.1016/j.bmcl.2018.09.031.

[13] S. Boutin, R. Maltais, J. Roy, D. Poirier, Synthesis of 17β-hydroxysteroid dehydrogenase type 10 steroidal inhibitors: Selectivity, metabolic stability and enhanced potency, European Journal of Medicinal Chemistry. 209 (2021) 112909. https://doi.org/10.1016/j.ejmech.2020.112909.

[14] Y. Xie, S. Deng, Z. Chen, S. Yan, D.W. Landry, Identification of small-molecule inhibitors of the Aβ–ABAD interaction, Bioorganic & Medicinal Chemistry Letters. 16 (2006) 4657–4660. https://doi.org/10.1016/j.bmcl.2006.05.099.

[15] K.R. Valasani, G. Hu, M.O. Chaney, S.S. Yan, Structure-Based Design and Synthesis of Benzothiazole Phosphonate Analogues with Inhibitors of Human ABAD-Aβ for Treatment of Alzheimer's Disease, Chemical Biology & Drug Design. 81 (2013) 238–249. https://doi.org/10.1111/cbdd.12068.

[16] K.R. Valasani, Q. Sun, G. Hu, J. Li, F. Du, Y. Guo, E.A. Carlson, X. Gan, S.S. Yan, Identification of Human ABAD Inhibitors for Rescuing Aβ-Mediated Mitochondrial Dysfunction, Curr Alzheimer Res. 11 (2014) 128–136. https://doi.org/10.2174/1567205011666140130150108.

[17] L. Hroch, O. Benek, P. Guest, L. Aitken, O. Soukup, J. Janockova, K. Musil, V. Dohnal, R. Dolezal, K. Kuca, T.K. Smith, F. Gunn-Moore, K. Musilek, Design, synthesis and in vitro evaluation of benzothiazole-based ureas as potential ABAD/17β-HSD10 modulators for Alzheimer's disease treatment, Bioorg. Med. Chem. Lett. 26 (2016) 3675–3678. https://doi.org/10.1016/j.bmcl.2016.05.087.

[18] L. Hroch, P. Guest, O. Benek, O. Soukup, J. Janockova, R. Dolezal, K. Kuca, L. Aitken, T.K. Smith, F. Gunn-Moore, D. Zala, R.R. Ramsay, K. Musilek, Synthesis and evaluation of frentizole-based indolyl thiourea analogues as MAO/ABAD inhibitors for Alzheimer's disease treatment, Bioorg. Med. Chem. 25 (2017) 1143–1152. https://doi.org/10.1016/j.bmc.2016.12.029.

[19] O. Benek, L. Hroch, L. Aitken, R. Dolezal, R. Hughes, P. Guest, M. Benkova, O. Soukup, K. Musil, K. Kuca, T.K. Smith, F. Gunn-Moore, K. Musilek, 6-Benzothiazolyl Ureas, Thioureas and Guanidines are Potent Inhibitors of ABAD/17 beta-HSD10 and Potential Drugs for Alzheimer's Disease Treatment: Design, Synthesis and in vitro Evaluation, Med. Chem. 13 (2017) 345–358. https://doi.org/10.2174/1573406413666170109142725.

[20] O. Benek, L. Hroch, L. Aitken, F. Gunn-Moore, L. Vinklarova, K. Kuca, D.I. Perez, C. Perez, A. Martinez, Z. Fisar, K. Musilek, 1-(Benzo[d]thiazol-2-yl)-3-phenylureas as dual inhibitors of casein kinase 1 and ABAD enzymes for treatment of neurodegenerative disorders, J Enzyme Inhib Med Chem. 33 (2018) 665–670. https://doi.org/10.1080/14756366.2018.1445736.

[21] L. Aitken, O. Benek, B.E. McKelvie, R.E. Hughes, L. Hroch, M. Schmidt, L.L. Major, L. Vinklarova, K. Kuca, T.K. Smith, K. Musilek, F.J. Gunn-Moore, Novel Benzothiazole-Based Ureas as 17β-HSD10 Inhibitors, A Potential Alzheimer's Disease Treatment, Molecules. 24 (2019) 2757. https://doi.org/10.3390/molecules24152757.

[22] M. Schmidt, O. Benek, L. Vinklarova, M. Hrabinova, L. Zemanova, M. Chribek, V. Kralova, L. Hroch, R. Dolezal, A. Lycka, L. Prchal, D. Jun, L. Aitken, F. Gunn-Moore, K. Kuca, K. Musilek, Benzothiazolyl Ureas are Low Micromolar and Uncompetitive Inhibitors of 17β-HSD10 with Implications to Alzheimer's Disease Treatment, International Journal of Molecular Sciences. 21 (2020) 2059. https://doi.org/10.3390/ijms21062059.

[23] T.T. Wager, X. Hou, P.R. Verhoest, A. Villalobos, Moving beyond Rules: The Development of a Central Nervous System Multiparameter Optimization (CNS MPO) Approach To Enable Alignment of Druglike Properties, ACS Chem. Neurosci. 1 (2010) 435–449. https://doi.org/10.1021/cn100008c.
[24] Z. Rankovic, CNS Drug Design: Balancing Physicochemical Properties for Optimal Brain Exposure, J. Med. Chem. 58 (2015) 2584–2608. https://doi.org/10.1021/jm501535r.
[25] PhysChem, ADME/Tox Calculations | ACD/Labs Percepta Software, (2020.1.2). https://www.acdlabs.com/products/percepta/index.php#resources (accessed April 6, 2020).
[26] R.Z. Cer, U. Mudunuri, R. Stephens, F.J. Lebeda, IC50-to-Ki: a web-based tool for converting IC50 to Ki values for inhibitors of enzyme activity and ligand binding, Nucleic Acids Res. 37 (2009) W441–W445. https://doi.org/10.1093/nar/gkp253.
[27] O. Trott, A.J. Olson, AutoDock Vina: improving the speed and accuracy of docking with a new scoring function, efficient optimization and multithreading, J Comput Chem. 31 (2010) 455–461. https://doi.org/10.1002/jcc.21334.
[28] Molecular Operating Environment (MOE), 2022.02 Chemical Computing Group ULC, 1010 Sherbooke St. West, Suite #910, Montreal, QC, Canada, H3A 2R7, 2023.
[29] P.A. Srere, [1] Citrate synthase: [EC 4.1.3.7. Citrate oxaloacetate-lyase (CoA-acetylating)], in: Methods in Enzymology, Academic Press, 1969: pp. 3–11. https://doi.org/10.1016/0076-6879(69)13005-0.
[30] J. Folbergrová, P. Ješina, R. Haugvicová, V. Lisý, J. Houštěk, Sustained deficiency of mitochondrial complex I activity during long periods of survival after seizures induced in immature rats by homocysteic acid, Neurochemistry International. 56 (2010) 394–403. https://doi.org/10.1016/j.neuint.2009.11.011.
[31] J. Hroudova, Z. Fisar, Activities of respiratory chain complexes and citrate synthase influenced by pharmacologically different antidepressants and mood stabilizers, Neuro Endocrinol Lett. 31 (2010) 336–342.
[32] M. Ľupták, Z. Fišar, J. Hroudová, Effect of Novel Antipsychotics on Energy Metabolism — In Vitro Study in Pig Brain Mitochondria, Mol Neurobiol. 58 (2021) 5548–5563. https://doi.org/10.1007/s12035-021-02498-4.
[33] Z. Fišar, K. Musílek, O. Benek, L. Hroch, L. Vinklářová, M. Schmidt, J. Hroudová, J. Raboch, Effects of novel 17β-hydroxysteroid dehydrogenase type 10 inhibitors on mitochondrial respiration, Toxicology Letters. 339 (2021) 12–19. https://doi.org/10.1016/j.toxlet.2020.12.012.
[34] Z. Fišar, Inhibition of monoamine oxidase activity by cannabinoids, Naunyn-Schmied Arch Pharmacol. 381 (2010) 563–572. https://doi.org/10.1007/s00210-010-0517-6.
[35] A.C. Tripathi, S. Upadhyay, S. Paliwal, S.K. Saraf, Privileged scaffolds as MAO inhibitors: Retrospect and prospects, European Journal of Medicinal Chemistry. 145 (2018) 445–497. https://doi.org/10.1016/j.ejmech.2018.01.003.
[36] O. Benek, O. Soukup, M. Pasdiorova, L. Hroch, V. Sepsova, P. Jost, M. Hrabinova, D. Jun, K. Kuca, D. Zala, R.R. Ramsay, J. Marco-Contelles, K. Musilek, Design, Synthesis and in vitro Evaluation of Indolotacrine Analogues as Multitarget-Directed Ligands for the Treatment of Alzheimer's Disease, ChemMedChem. 11 (2016) 1264–1269. https://doi.org/10.1002/cmdc.201500383.
[37] O. Benek, J. Korabecny, O. Soukup, A Perspective on Multi-target Drugs for Alzheimer's Disease, Trends in Pharmacological Sciences. 41 (2020) 434–445. https://doi.org/10.1016/j.tips.2020.04.008.
[38] F.H. Niesen, H. Berglund, M. Vedadi, The use of differential scanning fluorimetry to detect ligand interactions that promote protein stability, Nat Protoc. 2 (2007) 2212–2221. https://doi.org/10.1038/nprot.2007.321.
[39] L. Di, E.H. Kerns, K. Fan, O.J. McConnell, G.T. Carter, High throughput artificial membrane permeability assay for blood–brain barrier, European Journal of Medicinal Chemistry. 38 (2003) 223–232. https://doi.org/10.1016/S0223-5234(03)00012-6.

[40] V.N. Telvekar, H.M. Bachhav, V.K. Bairwa, A Novel System for the Synthesis of 2-Aminobenzthiazoles using Sodium Dichloroiodate, Synlett. 23 (2012) 2219–2222. https://doi.org/10.1055/s-0032-1317080.
[41] D.W. Engers, J.R. Field, U. Le, Y. Zhou, J.D. Bolinger, R. Zamorano, A.L. Blobaum, C.K. Jones, S. Jadhav, C.D. Weaver, P.J. Conn, C.W. Lindsley, C.M. Niswender, C.R. Hopkins, Discovery, Synthesis, and Structure−Activity Relationship Development of a Series of N-(4-Acetamido)phenylpicolinamides as Positive Allosteric Modulators of Metabotropic Glutamate Receptor 4 (mGlu4) with CNS Exposure in Rats, Journal of Medicinal Chemistry. 54 (2011) 1106–1110. https://doi.org/10.1021/jm101271s.
[42] D. Ménard, I. Niculescu-Duvaz, H.P. Dijkstra, D. Niculescu-Duvaz, B.M.J.M. Suijkerbuijk, A. Zambon, A. Nourry, E. Roman, L. Davies, H.A. Manne, F. Friedlos, R. Kirk, S. Whittaker, A. Gill, R.D. Taylor, R. Marais, C.J. Springer, Novel Potent BRAF Inhibitors: Toward 1 nM Compounds through Optimization of the Central Phenyl Ring, Journal of Medicinal Chemistry. 52 (2009) 3881–3891. https://doi.org/10.1021/jm900242c.
[43] M.D. Hanwell, D.E. Curtis, D.C. Lonie, T. Vandermeersch, E. Zurek, G.R. Hutchison, Avogadro: an advanced semantic chemical editor, visualization, and analysis platform, J Cheminform. 4 (2012) 17. https://doi.org/10.1186/1758-2946-4-17.
[44] E.F. Pettersen, T.D. Goddard, C.C. Huang, G.S. Couch, D.M. Greenblatt, E.C. Meng, T.E. Ferrin, UCSF Chimera—A visualization system for exploratory research and analysis, Journal of Computational Chemistry. 25 (2004) 1605–1612. https://doi.org/10.1002/jcc.20084.
[45] P.A. Ravindranath, S. Forli, D.S. Goodsell, A.J. Olson, M.F. Sanner, AutoDockFR: Advances in Protein-Ligand Docking with Explicitly Specified Binding Site Flexibility, PLOS Computational Biology. 11 (2015) e1004586. https://doi.org/10.1371/journal.pcbi.1004586.
[46] N.M. O'Boyle, M. Banck, C.A. James, C. Morley, T. Vandermeersch, G.R. Hutchison, Open Babel: An open chemical toolbox, J Cheminform. 3 (2011) 33. https://doi.org/10.1186/1758-2946-3-33.
[47] W. Humphrey, A. Dalke, K. Schulten, VMD: Visual molecular dynamics, Journal of Molecular Graphics. 14 (1996) 33–38. https://doi.org/10.1016/0263-7855(96)00018-5.
[48] J. Hroudová, Z. Fišar, Assessment of the Effects of Drugs on Mitochondrial Respiration, in: V. Weissig, M. Edeas (Eds.), Mitochondrial Medicine: Volume 3: Manipulating Mitochondria and Disease- Specific Approaches, Springer US, New York, NY, 2021: pp. 133–142. https://doi.org/10.1007/978-1-0716-1270-5_9.
[49] O. Lowry, N. Rosebrough, A. Farr, R. Randall, PROTEIN MEASUREMENT WITH THE FOLIN PHENOL REAGENT, Journal of Biological Chemistry. 193 (1951) 265–275. https://doi.org/10.1016/S0021-9258(19)52451-6.
[50] I.A. Trounce, Y.L. Kim, A.S. Jun, D.C. Wallace, [42] Assessment of mitochondrial oxidative phosphorylation in patient muscle biopsies, lymphoblasts, and transmitochondrial cell lines, in: Methods in Enzymology, Academic Press, 1996: pp. 484–509. https://doi.org/10.1016/S0076-6879(96)64044-0.
[51] D. Pesta, E. Gnaiger, High-Resolution Respirometry: OXPHOS Protocols for Human Cells and Permeabilized Fibers from Small Biopsies of Human Muscle, in: C.M. Palmeira, A.J. Moreno (Eds.), Mitochondrial Bioenergetics: Methods and Protocols, Humana Press, Totowa, NJ, 2012: pp. 25–58. https://doi.org/10.1007/978-1-61779-382-0_3.
[52] J. Čapek, M. Hauschke, L. Brůčková, T. Roušar, Comparison of glutathione levels measured using optimized monochlorobimane assay with those from ortho-phthalaldehyde assay in intact cells, Journal of Pharmacological and Toxicological Methods. 88 (2017) 40–45. https://doi.org/10.1016/j.vascn.2017.06.001.

**Highlights**

Fifteen new 17β-HSD10 inhibitors were designed, prepared, and evaluated.

Four submicromolar 17β-HSD10 inhibitors were identified (**6**, **9**, **11**, **12**).

Pharmacokinetic study after i.v. and p.o. administration was performed for **9** and **11**.

**Declaration of interests**

☐ The authors declare that they have no known competing financial interests or personal relationships that could have appeared to influence the work reported in this paper.

☒ The authors declare the following financial interests/personal relationships which may be considered as potential competing interests:

Ondrej Benek has patent #CZ307796 issued to University of Hradec Kralove. Kamil Musilek has patent #CZ307796 issued to University of Hradec Kralove. Lukas Hroch has patent #CZ307796 issued to University of Hradec Kralove.